Clim. Past, 8, 545–563, 2012
www.clim-past.net/8/545/2012/
doi:10.5194/cp-8-545-2012

Climate of the Past

Quantifying the ocean's role in glacial CO_2 reductions

M. O. Chikamoto[1], A. Abe-Ouchi[1,2], A. Oka[2], R. Ohgaito[1], and A. Timmermann[3]

[1]Research Institute for Global Change, Japan Agency for Marine-Earth Science and Technology, Yokohama, Kanagawa, Japan
[2]Atmosphere and Ocean Research Institute, University of Tokyo, Kashiwa, Chiba, Japan
[3]International Pacific Research Center, University of Hawaii, Honolulu, Hawaii, USA

Correspondence to: M. O. Chikamoto (megchika@jamstec.go.jp)

Received: 1 April 2011 – Published in Clim. Past Discuss.: 13 April 2011
Revised: 12 January 2012 – Accepted: 26 January 2012 – Published: 16 March 2012

Abstract. A series of Last Glacial Maximum (LGM) marine carbon cycle sensitivity experiments is conducted to test the effect of different physical processes, as simulated by two atmosphere-ocean general circulation model (AOGCM) experiments, on atmospheric pCO_2. One AOGCM solution exhibits an increase in North Atlantic Deep Water (NADW) formation under glacial conditions, whereas the other mimics an increase in Antarctic Bottom Water (AABW) associated with a weaker NADW. None of these sensitivity experiments reproduces the observed magnitude of glacial/interglacial pCO_2 changes. However, to explain the reconstructed vertical gradient of dissolved inorganic carbon (DIC) of 40 mmol m^{-3} a marked enhancement in AABW formation is required. Furthermore, for the enhanced AABW sensitivity experiment the simulated stable carbon isotope ratio ($\delta^{13}C$) decreases by 0.4 ‰ at intermediate depths in the South Atlantic in accordance with sedimentary evidence. The shift of deep and bottom water formation sites from the North Atlantic to the Southern Ocean increases the total preformed nutrient inventory, so that the lowered efficiency of Southern Ocean nutrient utilization in turn increases atmospheric pCO_2. This change eventually offsets the effect of an increased abyssal carbon pool due to stronger AABW formation. The effects of interhemispheric glacial sea-ice changes on atmospheric pCO_2 oppose each other. Whereas, extended sea-ice coverage in the Southern Hemisphere reduces the air-sea gas exchange of CO_2 in agreement with previous theoretical considerations, glacial advances of sea-ice in the Northern Hemisphere lead to a weakening of the oceanic carbon uptake through the physical pump. Due to enhanced gas solubility associated with lower sea surface temperature, both glacial experiments generate a reduction of atmospheric pCO_2 by about 20–23 ppmv. The sensitivity experiments presented here demonstrate the presence of compensating effects of different physical processes in the ocean on glacial CO_2 and the difficulty of finding a simple explanation of the glacial CO_2 problem by invoking ocean dynamical changes.

1 Introduction

During the late Pleistocene, the global temperatures and atmospheric carbon dioxide (CO_2) concentrations varied on 80–120 kyr glacial-interglacial timescale (e.g. Sigman et al., 2010; Fischer et al., 2010; Petit et al., 1999; Siegenthaler et al., 2005). Despite the prominent relationship between climate and the carbon cycle, the mechanisms controlling the glacial-interglacial pCO_2 variations are still unresolved (Sigman and Boyle, 2000; Archer et al., 2000). Compared to present-day conditions and as a result of more arid climate conditions and an extensive land ice coverage (Bird et al., 1994; Crowley, 1995), terrestrial carbon stocks were reduced considerably during glacial conditions. Accordingly, the marine carbon cycle must have been the main driver for lowering atmospheric pCO_2 by 80–100 ppmv during glacial periods.

There are several candidate mechanisms to explain the reduction in glacial atmospheric CO_2 levels (Archer et al., 2000; Sigman and Boyle, 2000; Köhler et al., 2005). One contributor to the glacial CO_2 decrease is an increase in the solubility of CO_2 gas (Bacastow and Maier-Reimer, 1990). It has been estimated that during glacial periods, a cooling of the surface oceans led to an atmospheric CO_2 drawdown of 25–30 ppmv through enhanced solubility in sea water (Sigman and Boyle, 2000; Kohfeld and Ridgwell, 2009). Because of the reduced vegetation, the remaining glacial-interglacial CO_2 difference is around 75 ppmv. Explaining the remaining 75 ppmv through ocean circulation changes has become a major challenge that has vexed the scientific community for years.

Based on paleo-proxy reconstructions it has been argued that the glacial ocean circulation state was significantly different from today's (Curry and Oppo, 2005; Lynch-Stieglitz et al., 2007). In the deep Southern Ocean, glacial pore waters were much more saline than today (Adkins et al., 2002), reflecting either a more sluggish Southern Ocean deep circulation (Lund et al., 2011) or reduced ventilation during the Last Glacial Maximum (LGM) (Skinner et al., 2010). The hypothesized reorganization of the large-scale ocean circulation has been suggested to affect the marine carbon cycle with implications for atmospheric pCO_2 changes (reviewed by Sigman et al., 2010). Model studies suggest that a weakening of vertical mixing around Antarctica may have contributed to a reduction of atmospheric CO_2 by over 20 ppmv (Toggweiler, 1999; Köhler et al., 2005; Peacock et al., 2006). These studies support the notion that lowering ventilation enhances deep-ocean stratification, leading to the sequestration of dissolved inorganic carbon (DIC) in the deep ocean. The stratification of the Southern Hemispheric water column is partly determined by local sea-ice conditions and sea-ice formation (Paillard and Parrenin, 2004; Watson and Naveira Garabato, 2006), partly by the water mass properties of Atlantic waters that upwell in the Southern Ocean. The latter can be affected by sea-ice conditions in the Northern Hemisphere, as suggested by Gildor et al. (2002). Hence we expect interplay between atmospheric CO_2 (determining the extend of the sea-ice), interhemispheric sea-ice changes (determining the level of CO_2 uptake through air-sea fluxes (Stephens and Keeling, 2000) and the level of mixing through brine release), and corresponding ocean circulation changes.

Changes in sea-ice coverage also affect biological productivity. An idealized linear increase in sea-ice extent shows the buildup of atmospheric CO_2 due to weakened biological productivity by light limitation (Archer et al., 2003; Kurahashi-Nakamura et al., 2007). A quantification of these interactions and their role in the glacial CO_2 response using a complex 3-dimensional climate-carbon cycle system model has hitherto not been performed.

Potential shifts of deep and bottom water formation from the North Atlantic to the Southern Ocean may lead to changes in the efficiency of oceanic carbon uptake by ocean biota (Ito and Follows, 2005). An increase in Southern Ocean bottom-water formation reorganizes the available utilized nutrients at the surface, weakening biological production and therefore oceanic carbon uptake (Marinov et al., 2008). These results suggest that an explicit representation of the deep-water formation in both polar regions may be an important element in the marine carbon cycle response to glacial-interglacial climate change.

The glacial-interglacial variability in atmospheric pCO_2 has been studied using idealized and/or glacial Sea Surface Temperature (SST) forcings in box-type (Hain et al., 2010) and intermediate complexity earth system models (Brovkin et al., 2007). Due to their low complexity and computational costs, these studies have explored a range of carbon-cycle responses, at the expense, however, of well-resolved physics. Moreover, sets of glacial-interglacial simulations using atmosphere-ocean general circulation models (AOGCM) have been carried out in Paleoclimate Model Intercomparison Project phase 2 (PMIP2). These experiments provide a deeper insight into interactions between ocean circulation and sea ice during the last glacial period.

To quantify the effects of glacial ocean circulation changes on the marine carbon cycle a hierarchy of models has been used, including box models, intermediate complexity models, and general circulation models (GCM) (Bopp et al., 2003; Tagliabue et al., 2009). In a recent study Tagliabue et al. (2009) found that reductions in deep water formation in both hemispheres are required to reproduce the reconstructed glacial special patterns of carbon isotope observations ($\delta^{13}C$ and $\Delta^{14}C$). However, the accompanied ocean biogeochemical change lowered atmospheric CO_2 by only 3 ppmv. Similar CO_2 changes have been reproduced in another GCM study (Bopp et al., 2003). In other words, the carbon isotope patterns do not provide enough constraints to reconstruct a glacial ocean circulation state that explain the lowering of the atmospheric pCO_2 concentrations by 80–100 ppmv.

In this study, we use a series of AOGCM simulations that represent glacial characteristics of different glacial ocean circulation states and sea-ice coverage and then evaluate the climate dynamical effects on the marine carbon cycle using an offline ocean biogeochemical model. The method applied here enables us to evaluate multiple simulations of the past and present ocean carbon cycle according to AOGCM climate simulations with low computational cost. Furthermore it enables us to isolate the individual effects of glacial ocean circulation, solubility and sea-ice coverage on atmospheric CO_2.

An earlier study has also attempted to evaluate the impact of individual climatic factors on the marine carbon cycle using idealized AMOC states (Cameron et al., 2005). We expand their approach by analyzing the atmospheric pCO_2 response to each factor of climate dynamics obtained from glacial AOGCM simulations.

2 Method

2.1 AOGCM and an offline biogeochemical model

We used an ocean biogeochemical model with an offline tracer advection scheme (Oka et al., 2008, 2011). A homogenized box atmosphere is coupled to a three-dimensional ocean biogeochemical model. In the tracer calculations, the model uses prescribed monthly climatology from 30-yr averages of horizontal ocean velocities, vertical diffusivity, sea surface height, sea surface wind speed, sea ice fraction, and sea-surface solar radiation, derived from a series of AOGCM experiments conducted with the Model for Interdisciplinary Research on Climate (MIROC) version 3.2

(K-1 model developers, 2004). These boundary conditions are interpolated from the $1.4^\circ \times 0.9^\circ$ averaged resolution of MIROC to 2.8° latitude $\times$ 2.8° longitude grids for the biogeochemical model to reduce computational cost (Oka et al., 2011). Meridional and zonal velocities are interpolated while preserving water volume flux at each grid. The other boundary conditions are linearly interpolated to the biogeochemical model grids. There are 44 vertical levels, which is the same resolution as that of MIROC.

The biogeochemical model is based on a simplified ecosystem of nutrient-phytoplankton-zooplankton-detritus (NPZD) ecosystem model (Plattner et al., 2001). The model includes two plankton functional groups of phytoplankton and zooplankton, suspended and sinking particulate detritus, four dissolved inorganic components of alkalinity, dissolved inorganic carbon (DIC), nitrate, and oxygen, and two carbon isotopes (^{13}C and ^{14}C). Biological production of particulate organic carbon (POC) depends on the available nitrate concentration and insolation based on Michaelis-Menten kinetics. The sinking rate of detritus is $8\,\mathrm{m\,day^{-1}}$ and the remineralization rate is $0.1\,\mathrm{day^{-1}}$ above 100 m and $0.02\,\mathrm{day^{-1}}$ below 100 m depth (Plattner et al., 2001). The production rate of calcium carbonate ($CaCO_3$) is assumed to be proportional to that of POC ($CaCO_3$:POC = 0.08) and the settling flux of particulate $CaCO_3$ in the water column decreases with an e-folding depth of 3500 m (Yamanaka and Tajika, 1996). The air-sea gas exchange of CO_2 is parameterized with a wind-speed dependent gas transfer coefficient (Wanninkhof, 1992). The oxygen gas exchange is determined by the temperature-dependent saturation state with respect to dissolved oxygen at the sea surface (Keeling et al., 1998). Atmospheric δ^{13}C and Δ^{14}C are set to -6.5 and 0 ‰, respectively. For comparisons of simulated δ^{13}C and Δ^{14}C patterns with proxy records, we additionally simulate the glacial ocean carbon cycle prescribed by atmospheric pCO$_2$ of 199 ppmv, δ^{13}C of -6.6 ‰, and Δ^{14}C of 0 ‰.

2.2 Experimental design

In this study, two pairs of preindustrial and glacial AOGCM simulations are used. The first set of preindustrial (PIa) and LGM (LGa) simulations contributed to PMIP2 intercomparison (Yanase and Abe-Ouchi, 2007; Otto-Bliesner et al., 2007). In the second pair of preindustrial (PIb) and LGM (LGb) experiments, we mimic the enhancement of AABW formation (Oka et al., 2011) according to proxy data that reconstruct the enhanced intrusion of AABW into the Atlantic basin (Duplessy et al., 1988; Sarnthein et al., 1994; Curry and Oppo, 2005) and model-comparison results that show a wide range of AABW feature in glacial simulations (Weber et al., 2007). In PIb and LGb, we have applied a form of flux adjustment in order to reduce a warm bias around Antarctica, as seen in the PMIP2 simulations. The current version in our model overestimates the incoming shortwave radiation in the Southern Ocean in associated with small cloud covers and then tends to have a warming bias (Watanabe et al., 2010). In order to remove this positive SST bias, we added to the calculated heat flux anomaly pattern with a cooling tendency that is latitudinally dependent and varies from $0\,\mathrm{W\,m^{-2}}$ at 45° S to $-15\,\mathrm{W\,m^{-2}}$ at 80° S. In addition, the coefficient of horizontal diffusion of the isopycnal layer thickness (an isopycnal/Gent-McWilliams (GM) eddy parameterization, Gent et al., 1995) was changed to the typical value for coarse-resolution model of $7.0 \times 10^{-6}\,\mathrm{cm^2\,s^{-1}}$ (Hirst and McDougall, 1996) from $3.0 \times 10^{-6}\,\mathrm{cm^2\,s^{-1}}$ (Gent et al., 1995; Watanabe et al., 2010) in the PIa and LGa versions. As a result of these changes SST reduces by 2.0–0.5 °C in the Southern Ocean and in the equatorial Pacific and in turns increases by 0.1–0.4 °C at 40° S and N (not shown). Both pairs of preindustrial and glacial experiments were conducted with the PMIP2 experimental protocol (Braconnot et al., 2007) with respect to continental ice sheet conditions (Peltier, 2004), trace gases, and Earth's orbital parameters (Berger, 1978). The AOGCM climatologies that are applied to the offline carbon cycle experiments are based on the last 30 yr of the MIROC 3.2 PIa, PIb, LGa, and LGb simulations.

To estimate the effects of enhanced Antarctic Bottom Water (AABW) formation on the marine carbon system under preindustrial conditions, we use the PIb climatology that is based on the last 30 yr of a 2019-yr-long integration under 1850 AD conditions. The additional surface heat flux forcing was applied after 1800 yr of the total integration. For LGb, the climatology from the last 30 yr of a 3029-yr integration under LGM condition is used. The additional heat flux forcing that leads to an enhancement of AABW formation was applied after 2700 yr of LGM integration. In all cases, we assume climatology as a steady-state system by repeating monthly climate conditions as forcing for the carbon cycle model. Interannual and longer-term climate variations are neglected in the off-line carbon cycle experiments.

The ocean carbon cycle simulations for both preindustrial experiments are spun up for 10 000 yr with prescribed atmospheric pCO$_2$ of 280 ppmv so that the solution can reach equilibrium in the atmospheric and oceanic carbon cycling. After 10 000 yr of integration, we diagnose the state of the preindustrial marine carbon cycle and of atmospheric pCO$_2$ variations. The carbon stored in the ocean reservoir amounts to 39 200 and 39 600 GtC in PIa and PIb, respectively. The glacial simulations LGa, LGb of the marine carbon cycle are run for 5000 yr starting from the equilibrated states of the preindustrial ocean carbon cycle experiments PIa, PIb, respectively. We analyze the response of the carbon cycle to the different physical forcings derived from the MIROC experiments.

2.3 Setup of factorial experiments

Idealized factorial model experiments are performed with the off-line carbon cycle model to separate the sensitivity of atmospheric pCO$_2$ with respect to changes in solubility, ocean

circulation, and sea-ice coverage in both Northern and Southern Hemispheres (Table 1). We conducted the factorial experiments for the "a" and "b" configurations and then drop these letters from the rest of the description (i.e. LGa-sl is identical to the LGa configuration and the solubility change). All factorial experiments except for LGa-oc use the glacial bathymetry. Experiment LGa-sl is identical to LGa, except that it uses the preindustrial SST, sea surface salinity (SSS), and wind speed in the off-line ecosystem model. In this case, the wind speed is used only for determining the air-sea gas exchange. The glacial simulations by MIROC neglect a 1-pus salinity increase due to 120 m depression of sea level. Therefore, the solubility effect includes reduced temperatures and the salinity change associated with LGM anomalies in evaporation and precipitation only. This experiment evaluates the anomalous solubility-induced pCO_2 fluxes into the atmosphere. Experiment LGa-in is similar to LGa, except that it uses the preindustrial sea-ice fraction and insolation in the Northern Hemisphere only. Note that this factorial experiment (LGa-in) isolates the effects of gas exchange and biological production due to sea-ice coverage, but does not include the ocean circulation change induced by the sea ice extent. The experiment focuses on the influence of the Northern Hemisphere sea ice on the ocean carbon cycle. Correspondingly, experiment LGa-is is obtained by modifying LGa to use the preindustrial Southern Hemisphere sea-ice fraction and insolation, and it is conducted to estimate the atmospheric pCO_2 response to the glacial sea ice in the Southern Ocean. Experiment LGa-oc is based on LGa, but it uses the preindustrial bathymetry, ocean vertical and horizontal velocities, sea surface height, vertical diffusivity, and oceanic interior temperature and salinity. This experiment can isolate the atmospheric pCO_2 sensitivity to the glacial ocean circulation. In the offline biogeochemical model, the isopycnal surfaces are recalculated using the temperature and salinity in the ocean interior, which affect the isopycnal mixing of tracers. Interior temperature and salinity fields are therefore applied only for tracer mixing along the isopycnal surface. These factorial experiments are run for 2000 yr, and they correspond to switching off individual glacial climatic factors. In the following we assess the carbon cycle differences between LGa (full glacial experiment) and each factorial experiment (Table 2).

In order to investigate the effects of glacial salinity, temperatures and wind speed on the CO_2 solubility, we conduct a second set of factorial experiments under preindustrial climate conditions (Table 1). The contributions of glacial solubility, ocean circulation, and sea ice in both hemispheres to atmospheric pCO_2 are estimated by the atmospheric pCO_2 difference from PIa in each factorial experiment (Table 2). Experiment PIa-sl is similar to the preindustrial experiments of PIa, but uses glacial SST, SSS and wind speed in the air-sea gas exchange parameterization. This experiment focuses on the glacial solubility effect in an interglacial environment. As well as LGa-sol, the solubility effects are responsible only for lowering surface temperatures and salinities due to the difference between precipitation and evaporation, but excluding the effect of the salinity increase caused by the build up of land ice. Experiment PIa-in is based on the PIa experiment but uses the glacial sea-ice concentration and insolation in the Northern Hemisphere. Similarly, experiment PIa-is is obtained from PIa, except that it uses the glacial sea-ice concentration and insolation in the Southern Hemisphere. These two experiments will help to quantify the atmospheric pCO_2 sensitivity to interglacial/glacial changes in sea-ice coverage and solar insolation in the Northern and Southern Hemispheres. Experiment PIa-oc is obtained from the preindustrial experiments, PIa, except that it uses the glacial bathymetry, ocean vertical and horizontal velocities, sea surface height, vertical diffusivity, and oceanic interior temperature and salinity. This experiment isolates the atmospheric pCO_2 response to the glacial ocean circulation under otherwise preindustrial boundary conditions. In the second set of experiments, all experiments use glacial sea surface area as bathymetry. In these experiments, the bathymetric change is considered to reflect the expanded ice sheet, which affects the total ocean surface area of air-sea interaction. The second set of factorial experiments corresponds to switching on the glacial climate factors under the modern background climate state. Factorial experiments of LGb simulation are also conducted, as well as factorial experiments of LGa. Comparison between results of the first and second factorial experiments allows us to evaluate the ocean carbon cycle dependence on the background state of climate.

3 Preindustrial and glacial marine carbon cycle simulations

3.1 Validation of present ocean carbon cycle simulation

The results of PIa and PIb are shown in Fig. 1. In both cases, the surface nitrate concentration is high in the Southern Ocean and the North Pacific (Fig. 1b and c), in accordance with observational data (Levitus et al., 1994) (Fig. 1a). The surface nutrient concentrations are underestimated in the eastern equatorial Pacific in both cases (Fig. 1b and c). In this study, we set the vertical velocity of particulate detritus lower than that of Plattner et al. (2001). The slower settling particulates contribute to more POC regeneration within the euphotic zone and maintains the surface nutrient compared to the nutrient distribution using the standard velocity (Plattner et al., 2001). The excess nitrate off the coast of Chile and in the Atlantic sector of the Southern Ocean is attributable to the deep-water supply via coastal upwelling or convective mixing.

Our model does not consider temperature-dependent biological production (Oschlies and Garcon, 1999) or temperature-dependent remineralization (Laws et al., 2000).

Table 1. Factorial experimental design and results.

Simulations	Changing parameters	pCO_2 ppmv	Solubility	N sea ice	S sea ice	Circulation
LGa	full	256.3	LGa	LGa	LGa	LGa
LGa-sl	solubility	285.6	PIa	LGa	LGa	LGa
LGa-in	N sea ice	252.2	LGa	PIa	LGa	LGa
LGa-is	S sea ice	260.2	LGa	LGa	PIa	LGa
LGa-oc	circulation	256.2	LGa	LGa	LGa	PIa
PIa	–	280.0	PIa	PIa	PIa	PIa
PIa-sl	solubility	251.2	LGa	PIa	PIa	PIa
PIa-in	N sea ice	284.6	PIa	LGa	PIa	PIa
PIa-is	S sea ice	277.0	PIa	PIa	LGa	PIa
PIa-oc	circulation	280.9	PIa	PIa	PIa	LGa
LGb	full	295.1	LGb	LGb	LGb	LGb
LGb-sl	solubility	294.8	PIb	LGb	LGb	LGb
LGb-in	N sea ice	252.1	LGb	PIb	LGb	LGb
LGb-is	S sea ice	266.2	LGb	LGb	PIb	LGb
LGb-oc	circulation	263.8	LGb	LGb	LGb	PIb
PIb	–	280.0	PIb	PIb	PIb	PIb
PIb-sl	solubility	243.0	LGb	PIb	PIb	PIb
PIb-in	N sea ice	296.5	PIb	LGb	PIb	PIb
PIb-is	S sea ice	282.7	PIb	PIb	LGb	PIb
PIb-oc	circulation	287.4	PIb	PIb	PIb	LGb

Table 2. How the climate factor contributions to the ocean carbon cycle are estimated.

Contribution factors	Glacial base	Preindustrial base
Solubility	LGa – LGa-sl	PIa-sl – PIa
N sea ice	LGa – LGa-in	PIa-in – PIa
S sea ice	LGa – LGa-is	PIa-is – PIa
Ocean circulation	LGa – LGa-oc	PIa-oc – PIa
Solubility	LGb – LGb-sl	PIb-sl – PIb
N sea ice	LGb – LGb-in	PIb-in – PIb
S sea ice	LGb – LGb-is	PIb-is – PIb
Ocean circulation	LGb – LGb-oc	PIb-oc – PIb

Consequently, SST in the Southern Ocean does not affect the nitrate distribution directly. Rather, it reflects the ocean circulation state and upwelling regions, with some sensitivity to the isopycnal/GM mixing parameterization.

The net primary production fluxes are 68.6 GtC yr^{-1} in PIa and 59.5 GtC yr^{-1} in PIb. These fluxes are larger than a recent satellite based estimate (48 GtC yr^{-1}, in Behrenfeld et al., 2006). The export fluxes of particulate organic matter of 10.5 and 10.4 GtC yr^{-1} in PIa and PIb (Fig. 1e and f) are in line with observationally-based estimates of 5–20 GtC yr^{-1} (Jahnke and Jahnke, 2004; Falkowski et al., 1998; Laws et al., 2000; Louanchi and Najjar, 2000).

The values of deep-water Δ^{14}C in the North Pacific reach −206 and −222 ‰ in PIa and PIb (Fig. 1h and i), respectively. These values are within the range of the regionally averaged value of −214 per mil from observational pre-bomb measurements (Key et al., 2004) (Fig. 1g). The values of deep-water Δ^{14}C in the North Pacific Ocean and the Southern Ocean in PIb are lower than the observational estimates. We attribute this to a lower radiocarbon value at the Southern Ocean surface in PIb compared with the observed radiocarbon data. This might be caused by the sea-ice coverage that decreases the sea surface radiocarbon values by preventing air-sea gas exchange of radiocarbon between atmosphere and ocean.

We estimate the preformed nutrient concentration indicating nutrient transport by ocean circulation as a conservative water-mass tracer (Ito and Follows, 2005). We simulate nitrate cycling of the ocean, but neglect denitrification and N_2 fixation processes. Therefore, the nitrate total inventory does not change in our model from Levitus World Ocean atlas (Levitus et al., 1994). In our model the simulated nitrate

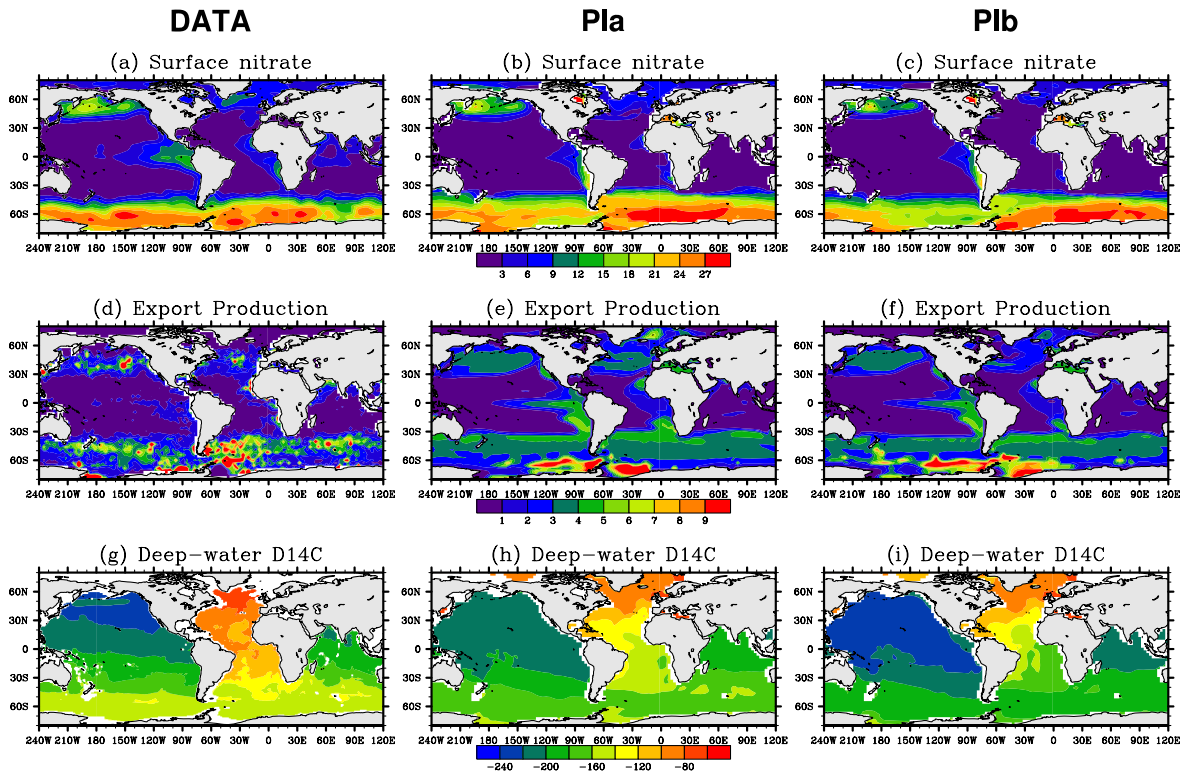

Fig. 1. Annual mean of nitrate concentration within the euphotic zone (mmol m^{-3}), export flux of POC (molC m^{-2} yr^{-1}) and radiocarbon below 1500 m (‰) for observational data (left panels), PIa (center), and PIb (right). Observational data refer to nitrate from Levitus World ocean atlas (Levitus et al., 1994). Export flux is estimated by Oka et al. (2008) based on the primary production algorithms (Behrenfeld and Falkowski, 1997) and the particle export ratios (Dunne et al., 2005). Natural radiocarbon data are taken from Global Ocean Data Analysis Project (Key et al., 2004).

concentration can be translated into phosphate concentration using a constant N:P stoichiometry (R_{NP}) of 14.21 based on the ratio of nitrate to phosphate in Levitus data. The preformed phosphate ([PO_4]*) is then calculated following Ito and Follows (2005) as

$$[PO_4]^* = ([NO_3] - [AOU] \times R_{NO}) \times R_{NP}. \quad (1)$$

Here, [NO_3] is the nitrate concentration, [AOU] is the utilized oxygen concentration (defined by [O_2]$_{sat}$-[O_2]), and R_{NO} is constant N:O_2 stoichiometry in our model (set to 8.526). The global-mean preformed phosphate concentrations are 1.05 and 0.75 µmol kg^{-1} in PIa and PIb, and the fractions of preformed phosphate to the global mean phosphate concentration (2.05 µmol kg^{-1}) are 0.49 and 0.30 in PIa and PIb, respectively. The value in PIa is close to the values of 0.46 using AOU concentration or 0.51 by the estimate of preformed phosphate concentration following Sarmiento and Gruber (2006) in Levitus data. The fraction of preformed phosphate concentration of 0.5 suggests that the ocean fills with a nearly equal mixture of waters below 1500 m produced in the Northern Atlantic and the Southern Ocean. The preindustrial condition in PIb, on the other hand, shows that deep waters are predominantly generated in the North Atlantic rather than in the Southern Ocean. From these results it becomes apparent that under preindustrial conditions the simulated distribution of biogeochemical tracers is sensitive to the heat flux forcing applied to the ocean and the GM parameterization.

3.2 Glacial climate simulations and the ocean carbon cycle

In LGa, North Atlantic Deep Water (NADW) formation is enhanced with respect to PIa (Fig. 2a and b). The maximum of NADW flow, defined by the maximum value of the Atlantic meridional stream function between 500 and 1500 m and 30° N to 50° N, increases by 5 Sv to 24 Sv. The maximum of AABW flow that is defined by the minimum value of the global meridional stream function at 3000 m depth is 10 Sv, which does not change with that in PIa. The resulting change in poleward heat transport in MIROC associated with the AMOC changes affects the SST and sea-ice extent in the North Atlantic (Fig. 3a and b).

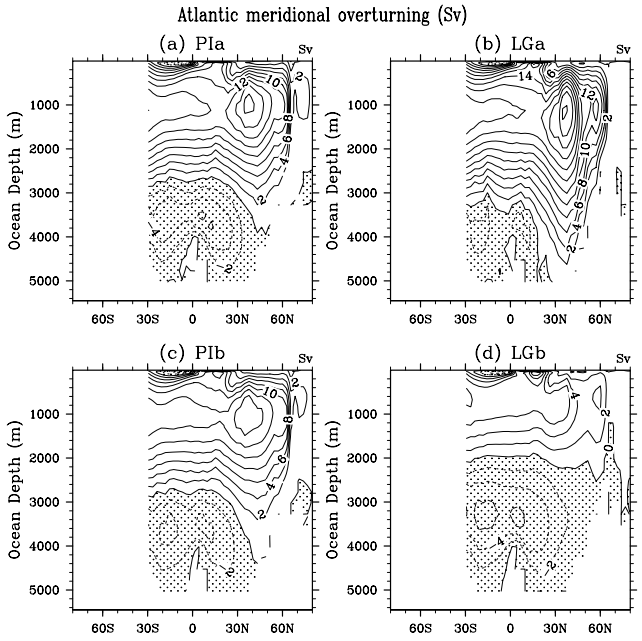

Fig. 2. Meridional overturning stream function (Sv) in the Atlantic Ocean of **(a)** PIa, **(b)** LGa, **(c)** PIb, and **(d)** LGb. Contour intervals are 2 Sv.

LGb exhibits an intensified AABW formation compared to PIb in association with the shoaling of NADW (Fig. 2d). The maximum of NADW flow in LGb decreases by 8 Sv to 8 Sv compared to PIb, and the AABW formation in turn increases by 2 Sv to 12 Sv. Southern Ocean and North Atlantic sea ice are found at lower latitudes in LGb than in LGa (Fig. 3). Compared to PIb, the average temperatures of Southern Ocean deep waters reduce by 1.5 °C in LGb (Fig. 4a and c), reaching levels near freezing point. In the tropical Atlantic, the bottom temperature in LGb decreases by 3.5 °C, corresponding to the oxygen isotope based reconstruction of deep water temperature during the last glacial maximum (Schrag et al., 1996). The average salinity increases in LGa and LGb (Fig. 4b and d), when considering the change in sea level applied to MIROC's output. We see in particular a large increase in salinity in AABW from PIb to LGb as a result of strong brine rejection in the Southern Ocean (Fig. 4d). The salinity change of 1.7 psu in the Southern Ocean is not enough to reconcile the glacial-interglacial variability in salinity by deep ocean proxy records (Adkins et al., 2002). The averaged potential density of the Southern Ocean deep water increases by 0.19 kg m^{-3} in LGa and 0.29 kg m^{-3} in LGb, which is dominated by higher salinity via brine rejection. Compared to LGa, AABW covers a larger volume of deep water in LGb. The simulated Southern Ocean sea ice in LGb is comparable to the observational data of September sea-ice distribution (Gersonde et al., 2005). On the other hand, the sea ice-covered area in the North Atlantic extends down to 40° N in LGb, which is an overestimation in comparison with sea-ice proxy data (Sarnthein et al., 2003).

To evaluate the glacial simulation using proxy records, we show the distribution of Δ^{14}C and δ^{13}C under the glacial climate conditions (Figs. 5 and 6). In the Southern Ocean in LGb, Δ^{14}C of the surface water decreases by 62 ‰ with respect to PIb through inhibiting air-sea gas exchange over the sea ice region (Fig. 5). The low-Δ^{14}C water is supplied to deep ocean, and expands to the North Atlantic Ocean. Greater reduction of radiocarbon of 100 ‰ is shown at intermediate depth in the North Atlantic by observations (Robinson et al., 2005), while LGb shows 36 ‰ reduction compared to PIb.

Similar, deep-water δ^{13}C decreases when NADW formation weakens and AABW formation strengths in LGb (Fig. 6). This case can reproduce the vertical and north-south gradients of carbon isotopes in the observations (Fig. 6b and e). The surface and deep δ^{13}C responses to the AMOC change from PIb to LGb are similar to the pattern in the prior study (Tagliabue et al., 2009), which is also consistent with proxy records (Fig. 6). However, whereas the maximum reduction of δ^{13}C by 0.4 ‰ appears in the Southern Ocean in our study, that appears in the North Atlantic Ocean in Tagliabue et al. (2009). The difference between two studies may be due to the balance between the northward transport of southern-origin waters and the slowdown of NADW (Hesse et al., 2011). Our results of low δ^{13}C water extent at the deep ocean can be found in a scenario that has an enhancement of AABW formation with an altered brine release with three-dimensional ocean circulation simulations (Hesse et al., 2011).

Associated with the enhanced NADW formation in LGa compared to PIa (Fig. 2b), DIC decreases by 32 mmol m^{-3} in the Atlantic deep water and increases by 28 mmol m^{-3} in the intermediate North Pacific water (Fig. 7a and b). The changes in carbon inventory are −60 GtC in the Atlantic, −3 GtC in the Southern, and +110 GtC in the Pacific Oceans. In LGa, nitrate increases at deep depth in the neither Pacific Ocean. This feature may originate from an anomalous meridional transport of increased unutilized nutrient of Antarctic waters. In contrast, LGb represented by a weakened NADW and an increased AABW reduces DIC by 32 mmol m^{-3} in the subsurface and increases by 17 mmol m^{-3} in the deep Atlantic Ocean (Fig. 7c). The carbon inventory is reduces by 7 GtC in the Atlantic Ocean and in turn increased by 17 and 33 GtC in the Southern and Pacific Oceans. The increase in vertical DIC gradient between the surface and deep water indicates the more effective storage of carbon in the abyssal ocean in LGb. This response is also present in the North Pacific Ocean (Fig. 7d).

Simulated changes in the overturning circulation (Fig. 2) affect also the nutrient distribution. The enhanced NADW formation in LGa compared to PIa increases the euphotic nitrate concentration in the North Atlantic Ocean (Fig. 8a). This means that the vigorous deep convection supplies nutrient-rich deep water to the surface. The increasing surface nutrient concentrations also appear in upwelling regions,

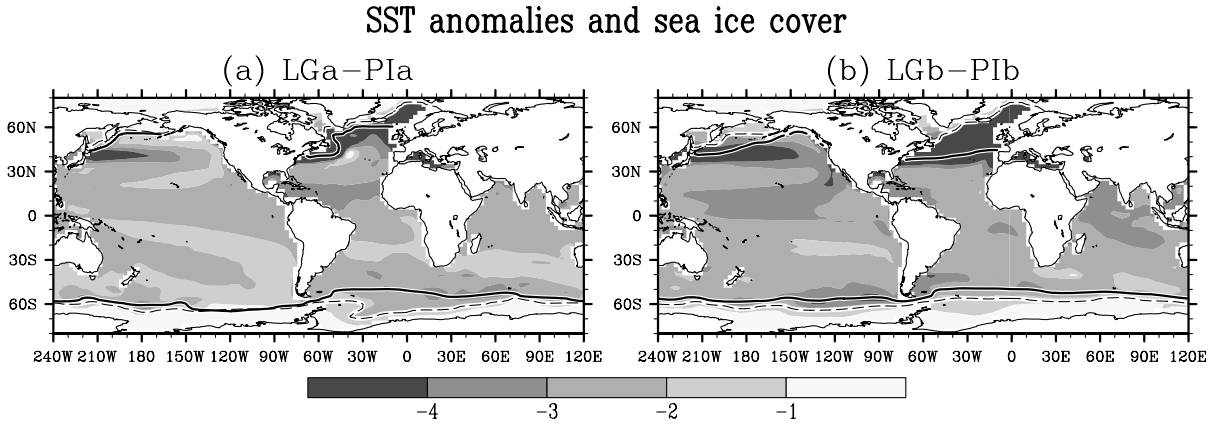

Fig. 3. SST anomaly (°C) **(a)** between LGa and PIa and **(b)** between LGb and PIb. Solid (dashed) lines show glacial (preindustrial) annual-mean sea ice fraction of 0.1.

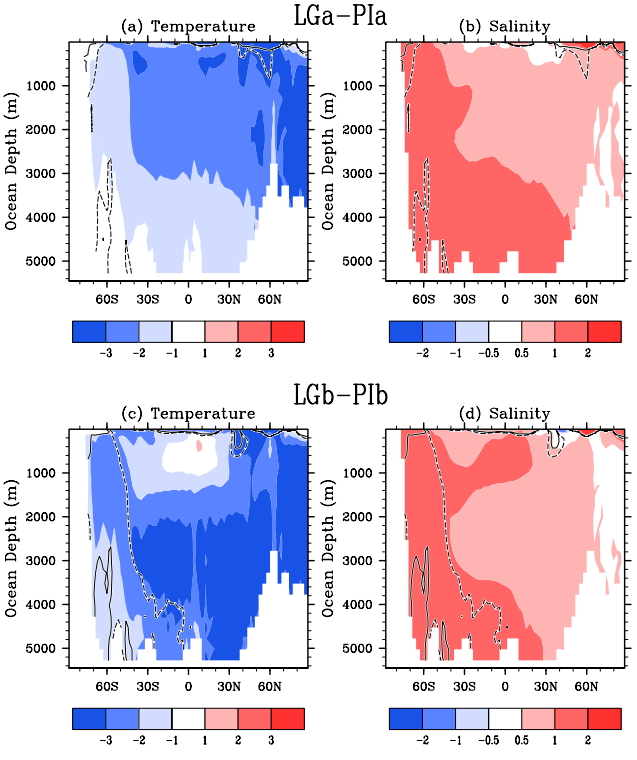

Fig. 4. Atlantic zonal-mean anomalies of potential temperature (°C) and salinity (psu) **(a** and **b)** between LGa and PIa and **(c** and **d)** between LGb and PIb. Salinity has been adjusted by 1 psu in each glacial AOGCM result to consider freshwater change due to frozen glacial ice sheets. Solid (dashed) lines indicate potential density anomaly of 0.35 (0.25) between each glacial and preindustrial simulations.

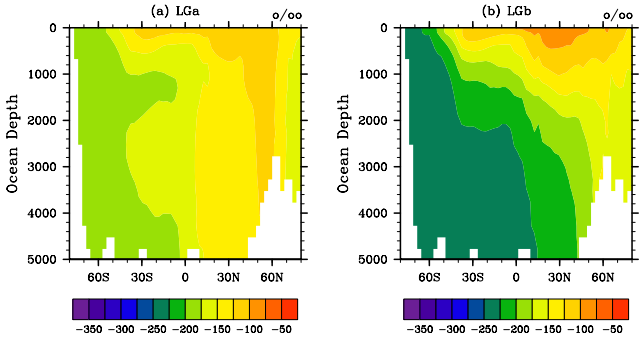

Fig. 5. **(a)** Atlantic Δ^{14}C (‰) in LGa. **(b)** as in **(a)**, but for in LGb.

such as the equatorial eastern Pacific and the western North Pacific Oceans. Along the sea ice margin, nutrients are supplied from the sea ice area (Fig. 8a) and biological production thus increases in the marginal sea ice zone (Fig. 8b). Biological production weakens under the sea ice region because the expanded sea ice prevents insolation from reaching the ocean surface. Global export flux of POC reduces by only −1.5 %. The oceanic carbon uptake is changed, as shown by the large anomalous air-sea CO_2 flux at high latitudes (Fig. 8c).

In LGb, the shift of deep water formation from the North Atlantic to the Southern Ocean accumulates DIC in the Atlantic deep water, which seems to be linked to the simulated δ^{13}C change (Fig. 6). The reduced ventilation associated with the weakening of NADW formation weakens the transport of nutrient-rich deep waters to the surface and reduces surface nitrate concentrations (Fig. 8d). The surface nutrient reduction weakens biological productivity globally (Fig. 8e), and the export flux of POC is reduced by 1.7 GtC yr^{-1}. The lack of an iron cycle in our marine carbon cycle model likely accounts for the underestimation in biological production around Antarctica compared with paleoproxy data

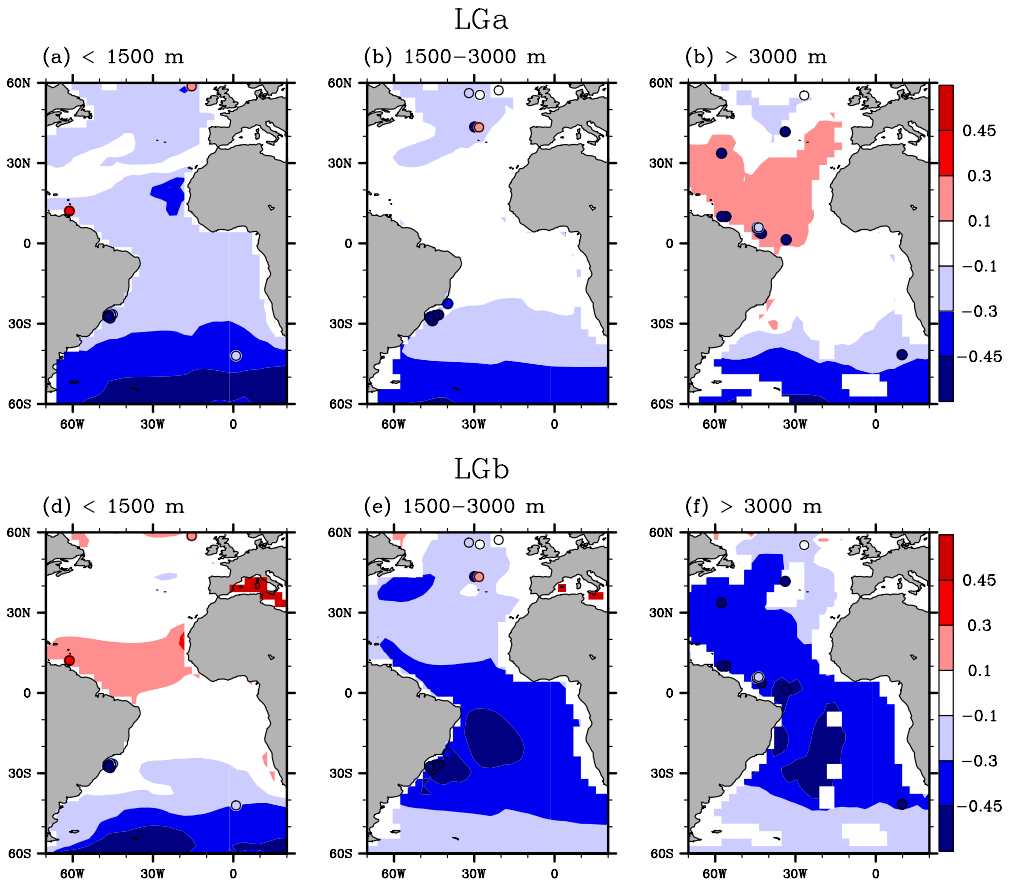

Fig. 6. **(a–c)** Atlantic δ^{13}C anomaly (‰) between LGa and PIa, averaged upper 1500 m depth, between 1500 and 3000 m, and below 3000 m. **(d–f)** as in **(a–c)**, but for between LGb and PIb. Circles are sediment core data (Curry and Oppo, 2005).

compilations (Bopp et al., 2003; Kohfeld et al., 2005; Oka et al., 2011). The air-sea CO_2 flux increases over the regions of annual sea ice coverage (Fig. 8f), which leads to a release of CO_2 from mixing of DIC-rich water. On the other hand, the air-sea CO_2 flux from the sea surface to the atmosphere reduces along the sea ice margin, thereby increasing the oceanic carbon uptake. The difference in responses of air-sea CO_2 gas exchange in the western North Pacific region of LGa and that of LGb may be affected by the deep-water circulation patterns that accompany carbon-rich water.

4 The effects of glacial climate factors on atmospheric pCO_2

Atmospheric pCO_2 is lowered by only 23.7 ppmv in LGa, while it is reduced by 20.0 ppmv in LGb (Fig. 9). These values are much smaller than the observed glacial-interglacial pCO_2 difference of 90 ppmv (which also includes a reduced land storage under glacial conditions). This may either suggest that the carbon cycle model is missing important components or that the simulated ocean circulation changes in MIROC are not adequate to generate a larger response in the carbon cycle. In this section we will try to disentangle the individual contributions to the glacial pCO_2 reduction and assess their uncertainties using a series of factorial sensitivity experiments (Tables 1 and 2). The sensitivities of atmospheric pCO_2 to gas solubility, ocean circulation, and sea-ice coverage in the Northern and Southern Hemispheres are summarized in Fig. 9. The pCO_2 responses to these individual climate factors are larger for LGb than for LGa. This is because the amplitudes of climate factor changes, such as sea surface temperature and sea ice extend, are larger in LGb than in LGa. In addition, the total sums of all factorial pCO_2 changes are different for the preindustrial and glacial basic state, indicating potential background state dependence of these sensitivities and potentially of climate carbon cycle feedbacks. Especially in LGb, the ocean carbon cycle appears to respond nonlinearly to a reorganization of ocean circulation in conjunction with large extent of sea ice. The total sum of the individual sensitivities are 27.5 ppmv in LGa and 23.8 ppmv in LGb, which is close to the LGa and LGb full experimental results that capture the combined effect of all forcings.

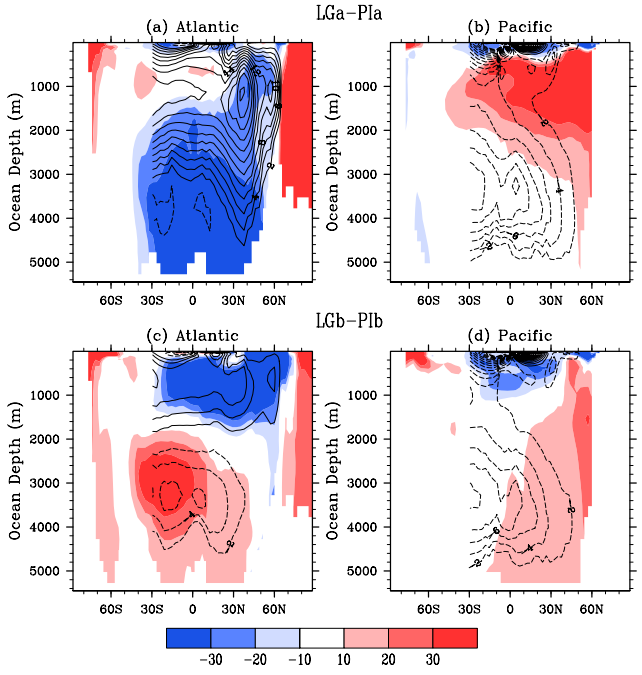

Fig. 7. Atlantic and Pacific DIC anomalies (mmol m^{-3}) **(a** and **b)** between LGa and PIa and **(c** and **d)** between LGb and PIb. Contour lines indicate the overturning stream function of each glacial simulation. Contour intervals are 2 Sv.

4.1 Solubility effect

The solubility change lowers atmospheric pCO_2 by 35.0 ppmv in LGb-sl (Fig. 9). Since the temperature change is larger in LGb than in LGa, the solubility effect is also larger in LGb-sl than in LGa-sl. The pCO_2 change contributes most significantly to the full glacial pCO_2 drop simulated in LGb. The solubility effect on atmospheric pCO_2 simulated here is larger than the upper bound of previous estimates of −30 ppmv according to intermediate complexity and GCMs models (Kohfeld and Ridgwell, 2009), suggesting that our model overestimates the solubility effect. This is because we do not consider the weakening of the solubility pump due to the glacial salinity increase of 1 psu. We estimate the effect of salinity on CO_2 solubility by a uniform addition of 1 psu to the glacial SSS and then obtain a 6-ppmv pCO_2 increase. This would bring the estimate of the combined solubility effect of temperature and salinity inside the range of previous estimates between −21 and −30 ppmv (Kohfeld and Ridgwell, 2009).

The atmospheric pCO_2 changes due to solubility under glacial and preindustrial background conditions (i.e. LGb-sl and PIb-sl) are quite similar (stars and circles in Fig. 9). DIC increases in the North Atlantic Ocean in both LGb-sl and PIb-sl (Fig. 10a and e). This suggests that the solubility is relatively independent of other climatic factors. The slightly smaller pCO_2 change in LGb-sl compared with that in PIb-sl could be related to the difference between sea ice coverage under glacial conditions and under preindustrial conditions. Since the expanded sea ice decreases the area of outcropping cold water, ocean carbon uptake is reduced at high-latitudes (Fig. 11a and e). Also, our results suggest that the effects of temperature and salinity on air-sea gas exchange are roughly equal even if the ocean interior temperature and salinity are different between the preindustrial and the LGM state. The ocean interior temperature and salinity are used for the calculation of the ocean interior CO_2 solubility and isopycnal mixing in our model. Therefore, these processes have a small impact on the atmospheric pCO_2 when the sea-level driven salinity change is not considered.

4.2 Sea ice coverage in the Northern Hemisphere

In LGb-in the glacial increase in sea ice area in the Northern Hemisphere increases atmospheric pCO_2 (Fig. 9), because the sea ice in the northern North Atlantic prevents oceanic carbon uptake through gas solubility. The weakening of gas solubility in the northern area obviously reduces DIC of the whole Atlantic Ocean (Fig. 10b).

Similarly, atmospheric pCO_2 increases in PIb-in. The large difference in DIC between LGb-in and PIb-in emerges at intermediate depths in the North Atlantic (Fig. 10b and f). The ocean circulation in PIb-in corresponds to vigorous preindustrial AMOC. Since NADW is characterized by DIC-poor water compared to AABW, the more dominant mode of NADW reduces DIC preservation over the North Atlantic Ocean (Fig. 10b and f). As a result, the amplitude of the atmospheric pCO_2 rise is larger in PIb than in LGb.

The sea ice cover weakens biological production, because it reduces the penetration of solar irradiance into the ocean. Contrasting this effect, biological production increases along the sea-ice margin as unutilized nutrients are supplied to the open ocean. Consequently, biological production does not change atmospheric pCO_2 considerably.

4.3 Sea ice coverage in the Southern Hemisphere

In contrast to the sea-ice coverage in the Northern Hemisphere, the glacial sea ice in the Southern Hemisphere reduces atmospheric pCO_2 by 6.2 ppmv (Fig. 9). The sea-ice coverage extends over the upwelling region of the Southern Ocean, and the air-sea gas exchange close to Antarctica is decreased (Fig. 11c). This result suggests that the sea ice change in the Southern Ocean inhibits CO_2 release into the atmosphere, but to a lesser extent than proposed by Stephens and Keeling (2000). In Stephens and Keeling (2000), atmospheric pCO_2 drastically decreases by over 10 ppmv only when the sea ice area approaches at least 96 % south of the Antarctic Polar Front (APF). On the other hand, our simulation shows the area of annual-mean sea ice coverage reaches to 2.0×10^{13} m^2, which is 85 % for the ocean area south of 60° S (2.3×10^{13} m^2). Indeed the atmospheric pCO_2 change

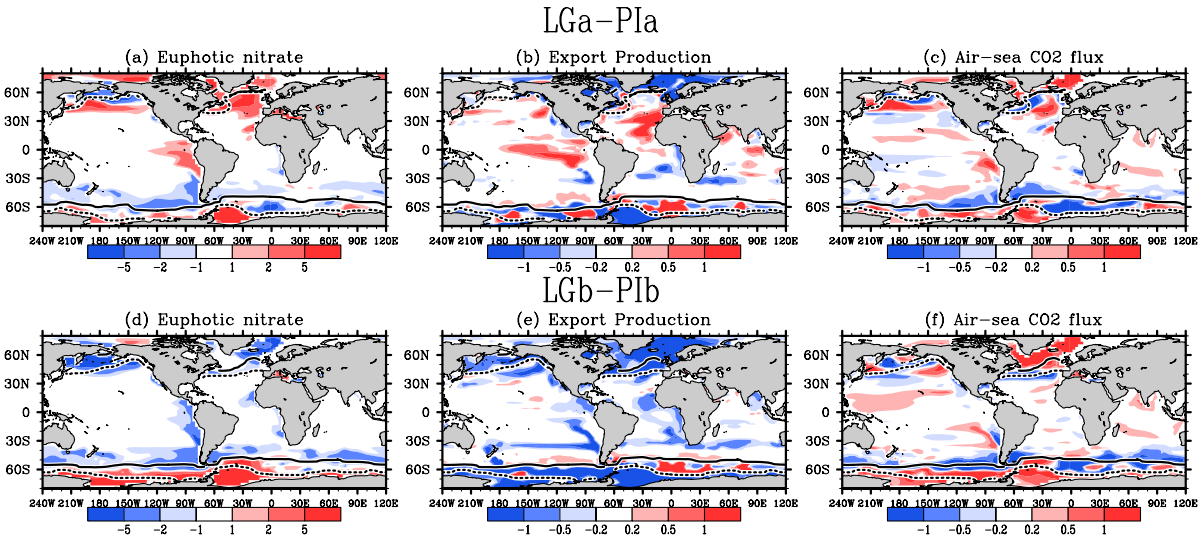

Fig. 8. Annual-mean euphotic averaged nitrate anomaly (mmol m^{-3}), export POC anomaly (molC m^{-2} yr^{-1}), and air-sea CO_2 flux anomaly (mol m^{-2} yr^{-1}) **(a–c)** between LGa and PIa and **(d–f)** between LGb and PIb. Solid (dotted) lines refer to glacial sea ice fraction of 0.1 in August (February).

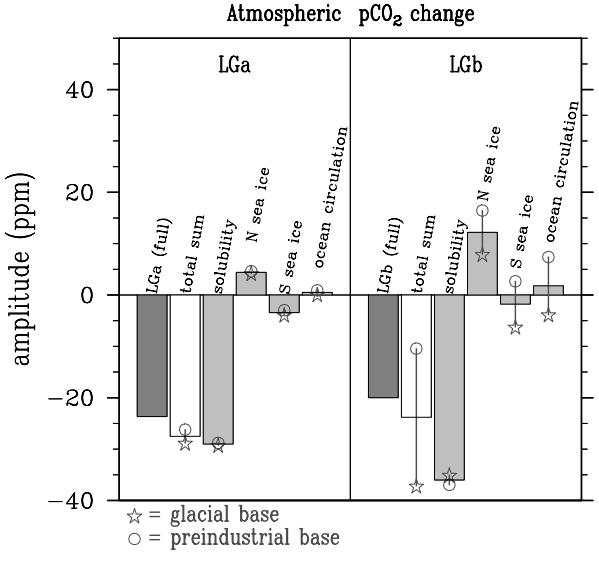

Fig. 9. Atmospheric pCO_2 responses to the climate dynamic changes. The left panel shows configuration "a" experiments, which switch on or off the climate factors of LGa. The right panel is the same in the left, but for configuration "b" experiments, switching on/off the climate factors of LGb. Thick bars refer to the average of two factorial estimates in the glacial and preindustrial climates (Table 1).

is consistent with that in the 85 % case in Stephens and Keeling (2000). The fraction of sea-ice coverage to the ice free area south of APF would affect the atmospheric pCO_2 change.

In addition, light limitation in the extended glacial perennial sea-ice region reduces biological production: primary production drops by 36 % south of 60° S and export production decreases by 36 % as well. Biological production near the marginal sea-ice zone in turn increases due to the nutrient supply from the permanent sea ice region. Together, these processes result in a 4.2 % decrease of global export flux of POC. The northward shift of biological productivity and the biological production change are agreement with the glacial simulation by Menviel et al. (2008a), which is also consistent with the proxy records of nutrient concentration (Elderfield and Rickaby, 2000) and primary production (Kohfeld et al., 2005). The pCO_2 lowering as a result of reduced CO_2 degassing in the polar region partly counteracts the pCO_2 rise through the weakening of biological production. The opposing effects of physical and biological processes on atmospheric pCO_2 support results from a coupled climate-carbon simulation study (Kurahashi-Nakamura et al., 2007).

4.4 Ocean circulation

The glacial ocean circulation state increases DIC at intermediate depth in 30° S relative to the pre-industrial base experiment in both LGb-oc and PIb-oc (Fig. 10d and h). Since this increase is found in both present and glacial sea-ice conditions (PIb-oc and LGb-oc) (Fig. 10h), the carbon storage in the abyssal ocean is due to the enhancement of AABW formation. Despite these large-scale responses, the sensitivity

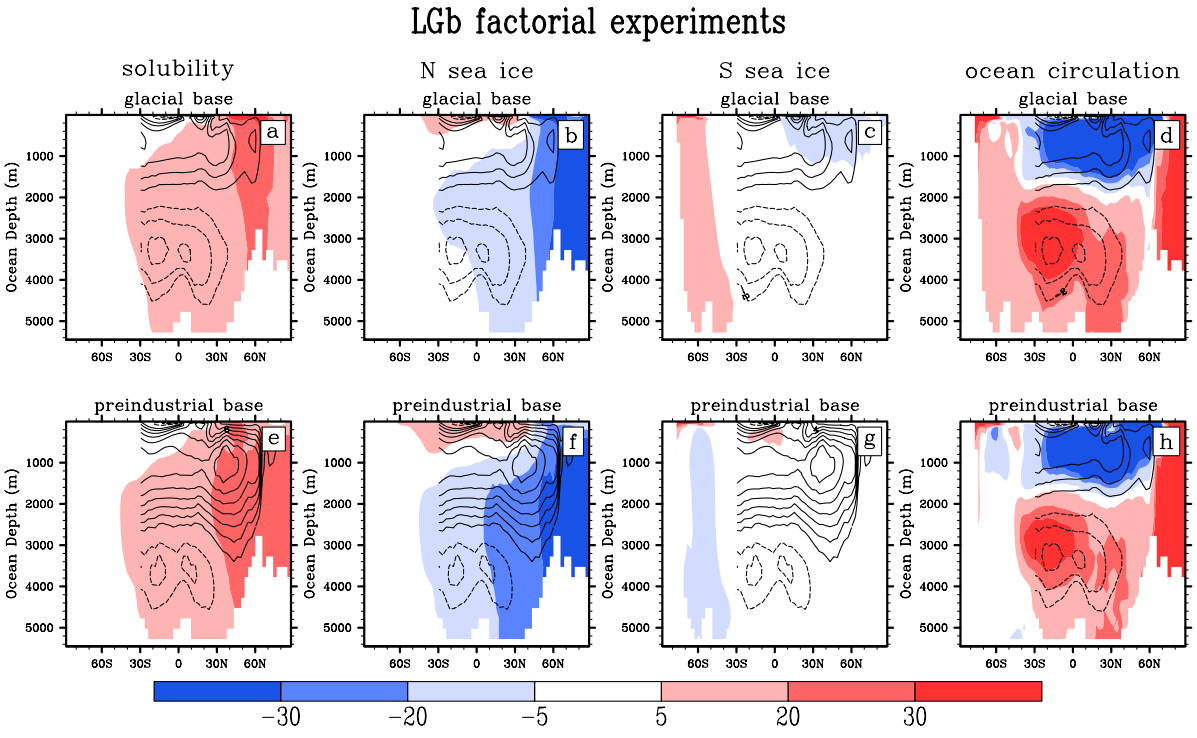

Fig. 10. Zonal-mean DIC anomalies (mmol m^{-3}) due to changes in the solubility, sea ice in the Northern and Southern Hemispheres, and ocean circulation of LGb. Upper (lower) panels correspond to results from the glacial (preindustrial) based climate. Contour lines indicate the overturning stream function of each factorial experiment. Contour intervals are 2 Sv.

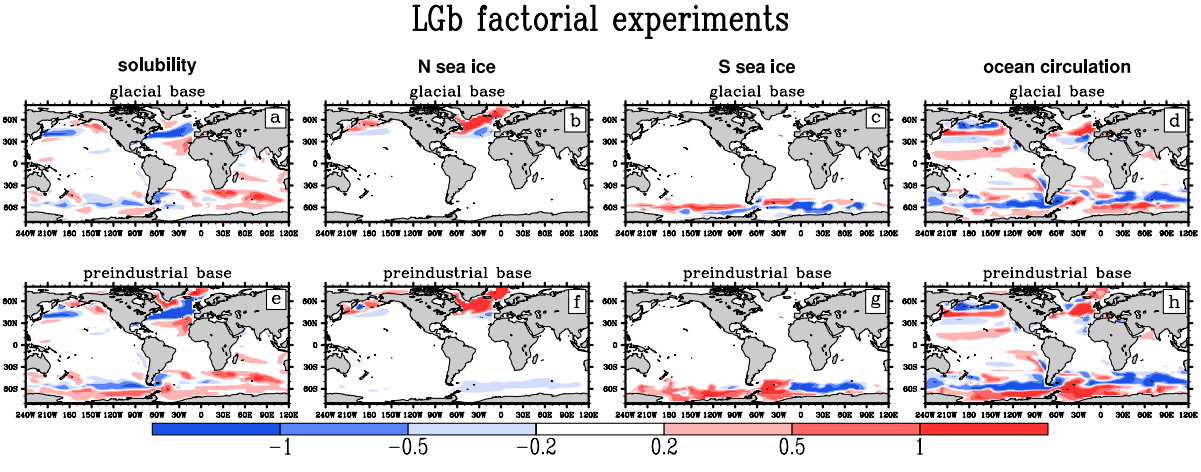

Fig. 11. Anomalous air-sea CO_2 flux (mol m^{-2} yr^{-1}) due to changes in the solubility, sea ice in the Northern and Southern Hemispheres, and ocean circulation of LGb. Upper and lower panels are as in Fig. 10.

of atmospheric pCO_2 to the glacial/interglacial ocean circulation changes amounts to only −3.8 ppmv in LGb-oc.

The dominance of AABW formation over NADW formation in LGb would change the oceanic carbon uptake via biota around Antarctica, as shown by the anomalous CO_2 flux in the Southern Ocean (Fig. 11d). Indeed the enhancement of AABW in LGb accompanies to an increase in preformed phosphate in the Southern Ocean (Fig. 12). The fraction of global-mean preformed phosphate to the global-mean phosphate concentration increases by 0.027 in LGa from LGa-oc and 0.033 in LGb from LGb-oc. According to Ito and Follows (2005), the increase in preformed nutrients means that the biological carbon uptake weakens, thereby increasing atmospheric pCO_2. Therefore our results suggest that the atmospheric pCO_2 reduction due to increased carbon storage in AABW may offset the atmospheric pCO_2 rise due to reduced biological production. It should be noted, however, that the estimate of preformed nutrient concentrations is sensitive to the surface oxygen concentration in polar regions, so that the comparison between the preindustrial and glacial states must be interpreted with caution. In addition, a significant increase in dust deposition in the Southern Ocean affects biological productivity directly (Martin, 1990). In this case, the biological change itself can reduce the atmospheric pCO_2 (e.g. Hain et al., 2010; Oka et al., 2011). This effect can be larger than the effect of nutrient redistribution through southern deep- and bottom-water forming.

To analyze the effect of ocean circulation changes on marine geochemistry, we examine the differences in the zonally-averaged ocean surface DIC (ΔDIC), alkalinity (ΔALK), pH (ΔpH), and CO_2 concentration (ΔCO_2) due to the imposed glacial-interglacial ocean circulation change (Fig. 13). In this study, the total oceanic-atmosphere carbon inventory is stable, as we neglect the global carbon budget change through sedimentation processes and changes in land weathering processes. This means that our estimate in this study is subject to the oceanic chemistry change induced only by climatic factors.

The weakening of NADW formation reduces ΔDIC and ΔALK significantly in the entire North Atlantic (Fig. 13a). In turn, ΔDIC and ΔALK increase south of 60° S because the upwelled carbon-rich deep waters stay below the sea ice area.

It should be noted here that the glacial ocean circulation alters ΔDIC and ΔALK simultaneously in the Atlantic and Pacific basins (Fig. 13a and b). Therefore these changes cause only a small change in surface pH and thus reduce atmospheric pCO_2 only slightly (Fig. 13c and d). Especially at low latitudes, simultaneously occurring anomalies in DIC and alkalinity do not change the surface pH and then CO_2 concentration. A decrease in ΔDIC that was greater than that in ΔALK would increase pH and greatly reduce atmospheric pCO_2. The simulated small difference between ΔDIC and ΔALK in our glacial experiment consequently leads to a small reduction in atmospheric CO_2.

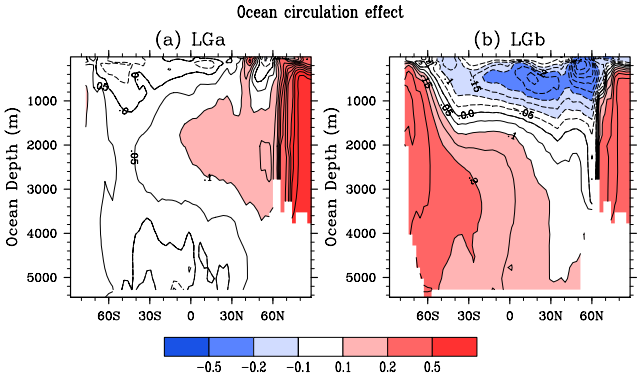

Fig. 12. Global zonal-mean preformed phosphate anomalies (μmol kg^{-1}) due to ocean circulation change **(a)** between LGa and LGa-oc and **(b)** between LGb and LGb-oc.

The meridional variations in carbon storage affect the atmospheric CO_2 sensitivity as well. The carbon accumulation increases in the South Atlantic, but decreases in the North Atlantic. In the Southern Ocean, an enhancement of carbon-rich AABW carries carbon to the deep ocean. The southern sea ice also contributes to the carbon pool through inhibiting the CO_2 gas release. However, in the North Atlantic, sea ice coverage reduces carbon uptake, thereby reducing DIC by 4 TgC (Fig. 13e). The North Atlantic sea ice counteracts the effects of carbon accumulation in the Southern Ocean due to increased AABW formation and the Southern Hemisphere sea ice coverage.

These glacial simulations do not consider the salinity increase induced by the drop in global sea-level that is expected to cause further reorganizations of the ocean circulation. If we consider a salinity increase associated with the glacial sea-level drop, the glacial ocean circulation has the potential to amplify the atmospheric pCO_2 reduction by 10 ppmv (−4 ppmv by ocean circulation and −6 ppmv by sea-level driven solubility). Earth system models that capture vegetation, ocean circulation changes, sea ice coverage, and sea level changes associated with land ice build up would help to further contribute to our understanding of the contributors to the glacial atmospheric CO_2 reduction.

5 Discussion

5.1 Carbon storage response to AABW changes

The strength and structure of NADW formation are connected to the strength of AABW formation; the export of NADW into the Southern Ocean partly controls the vertical density structure in the AABW formation regions, which translates into changes of AABW production. Our LGb experiment exhibits a weakening of NADW formation and an increase in AABW volume for the glacial climate state. The weakening of NADW formation reduces northward heat

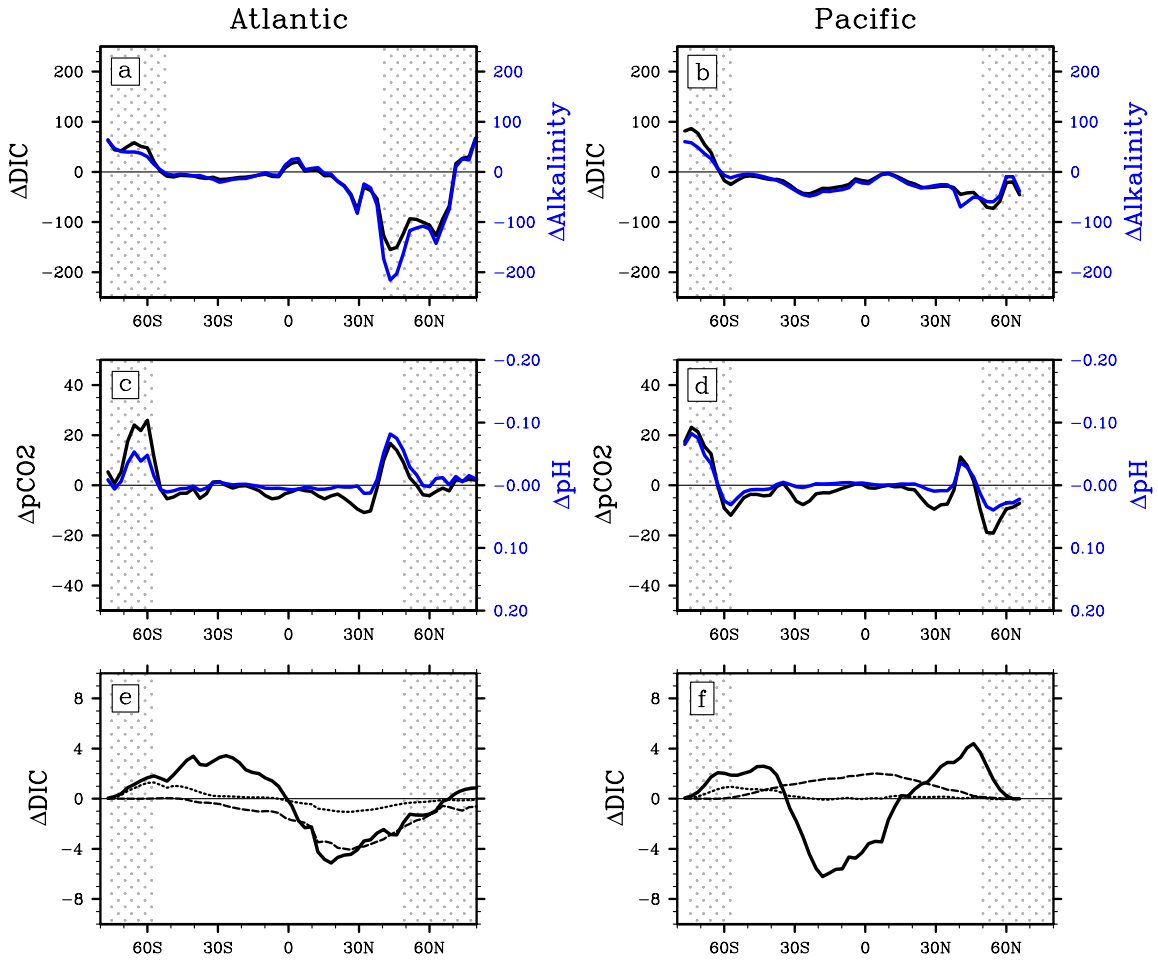

Fig. 13. (**a** and **b**) Zonal-mean ocean surface alkalinity (black) and DIC (mmol m^{-3}) (gray) difference between LGb and LGb-oc in the Atlantic and Pacific Ocean. Panels (**c** and **d**) are the same as (**a** and **b**) except ocean surface CO_2 concentration (ppmv) (black) and pH (gray) anomalies are weighted by the cosine of the latitude. Panels **(e** and **f)** are zonal-integrated DIC accumulation changes (TgC) due to ocean circulation (solid), the northern sea ice (dashed), and the southern sea ice (dotted). Dotted areas indicate the sea ice fraction of over 0.1 in LGb.

transport in the Atlantic Ocean. The glacial ocean circulation seems to be determined by the balance between thermal buoyancy fluxes at northern high latitudes and haline buoyancy fluxes at southern high latitudes, as discussed by Gildor et al. (2002). However, the salinity increase of 1.7 psu in the Southern Ocean deep water is not enough to justify the glacial proxy data variability by 2.4 psu at a single deep-depth core of the Southern Ocean (Adkins et al., 2002). Although our analysis cannot distinguish between the haline and thermal effects on ocean circulation and resulting glacial-interglacial CO_2 changes, it is qualitatively supporting the notion that denser AABW will provide a means to sequester atmospheric CO_2 during glacial condition (Bouttes et al., 2010).

Our study shows a small sensitivity of atmospheric pCO_2 to glacial-interglacial ocean circulation changes, which agrees with the previous GCM results (Bopp et al., 2003; Tagliabue et al., 2009). The small sensitivity of atmospheric CO_2 to glacial boundary conditions seems to be a general feature in present GCM studies. A larger sensitivity was recently described in an EMIC study (e.g. Brovkin et al., 2007). One of the key differences between Brovkin et al. (2007) and our study is related to the glacial salinity change and the associated DIC increases south of 40° S. As shown by the vertical uniformed changes in $\delta^{13}C$ and DIC south of 40° S (Figs. 6 and 7c), the Southern Ocean stratification would even weaken in LGb. Indeed in our model, the dense water that is produced near sea-ice margin via brine rejection accompanies to the density-induced deep convection. These features would contribute to the CO_2 release from the ocean to the atmosphere through mixture of surface and deep

water, thereby offsetting to the effect of carbon storage by the AABW formation. This supports again the idea that the pattern of stratification changes in the Northern and Southern Hemisphere plays a key role in controlling glacial pCO_2.

Furthermore, such differences could also be related to the fact that simplified two-dimensional ocean models, as used by Brovkin et al. (2007), can not resolve the full 3-dimensional structure of the ocean which may be important in the biogeochemical response to LGM climate change (Bouttes et al., 2009). Horizontal effects may affect the distribution of DIC at the surface. Also, the established Southern Ocean bottom water formation in our model is substantially different from box model studies (Watson and Naveira Garabato, 2006; Paillard and Parrenin, 2004), which have argued that a large reduction in atmospheric pCO_2 results from enhanced stratification of the Southern Ocean. The box models tend to simulate a larger high-latitude sensitivity of pCO_2 to climate forcing compared with GCMs, because they have a larger outcropping area in the polar region (Bacastow, 1996; Archer et al., 2000; Broecker et al., 1999).

Potential shifts in the regions of deep- and bottom-water replenishment from the North Atlantic to the Southern Ocean could change the strength of biological pump in the ocean. Toggweiler et al. (2003) argued that the increase in Southern Ocean deep-water formation weakens biological production through utilized nutrient redistribution, thereby changing the atmospheric pCO_2 response to the ocean circulation change. In LGb, the fraction of preformed nutrients to the total nutrient increases by a small factor of 0.033. Following the simplified estimate of the atmospheric pCO_2 change from the fraction change (Ito and Follows, 2005), the atmospheric pCO_2 change is +10 ppmv due to biological efficiency. The reorganization of the Southern Ocean causes carbon storage and redistribution of nutrients, but these effects on atmospheric pCO_2 tend to cancel out. This estimate should be done with caution because the biological process change is thought to be primary driver of atmospheric pCO_2. On the other hand, there is another perspective on a Southern Ocean nutrient and carbon distributions, which is controlled by the Southern Ocean dynamics (e.g. Toggweiler et al., 2006). They argue that atmospheric pCO_2 is determined by how fast the ventilated southern water with rich-nutrient and carbon water sinks back into deep ocean, and this accompanies corresponding changes in marine biological productivity.

In this study, we show that the current states of marine carbon inventory are quite different between PIa and PIb. When we simulated the ocean carbon cycle using LGb climate state but starting from the PIa carbon field, atmospheric pCO_2 reduces by 42 ppmv. This change is larger than that in LGb, suggesting the initial state of carbon pool affects the atmospheric pCO_2 change. When comparing multi-model studies, how much the initial carbon is pooled in the ocean would be also important to evaluate the atmospheric pCO_2 sensitivity.

5.2 Potential of ocean biogeochemical effects on atmospheric pCO_2

The glacial ocean circulation drives DIC and alkalinity anomalies simultaneously (Fig. 13), leading to a relatively small reduction in surface pH and ocean surface pCO_2. The simultaneous carbon chemistry changes might be due to the simplified biogeochemistry whereby the model assumes constant export ration ratio and settling rate of particles everywhere. The water temperature dependence of phytoplankton growth (Eppley, 1972), remineralization (Matsumoto, 2007), and calcification rate (Maier-Reimer and Bacastow, 1990) may add new sensitivities to the marine carbon cycle's response to LGM climate change that need to be further assessed in future work. The marked reduction in NADW in LGb accounts only for a small reduction in surface pH (Fig. 13), because our simulation assumes a stable total carbon budget in the atmosphere and ocean systems as a closed system (Sigman et al., 1998). If we consider the variability in total carbon budget as a result of sedimentation process changes, atmospheric pCO_2 can change largely through variability in oceanic carbon and alkalinity inventories (e.g. Chikamoto et al., 2009). For example, when the deep water stores large quantities of carbon and becomes more acidic under glacial ocean circulation conditions (Brovkin et al., 2007) or when the AMOC collapses (Chikamoto et al., 2008), atmospheric pCO_2 further decreases due to carbonate compensation. In fact, our glacial experiment shows that the enhanced AABW formation carries carbon-rich water in the abyssal Atlantic Ocean and then causes acidification of the overlying bottom water (not shown). This condition would potentially drive pH largely through carbonate compensation and the associated pCO_2 reduction.

During the glacial periods, dust deposition was considerably higher than today (e.g. Petit et al., 1999), which would contribute to biological productivity in the nutrient-rich low-chlorophyll region, such as the Southern Ocean (Martin, 1990). Some model studies show iron fertilization enhances biological production and hence reduces atmospheric pCO_2 by 8–40 ppmv (Watson et al., 2000; Archer et al., 2000; Bopp et al., 2003). In MIROC experiment LGb, the glacial dust deposition lowers atmospheric pCO_2 by 42 ppmv (Oka et al., 2011), suggesting that atmospheric pCO_2 can be further reduced due to the altered biological productivity through iron fertilization.

5.3 Glacial westerlies

Toggweiler et al. (2006) proposed that possible glacial shifts of southern hemispheric westerlies may affect the strength and position of upwelling around Antarctica. Moreover, this shift as indirectly inferred from changes in biogenic silica in few core sites in the Southern Ocean during the last glacial termination correlates well with the timing of the atmospheric pCO_2 rise (Anderson et al., 2009). The change in

wind-driven Southern ocean overturning would affect atmospheric pCO_2 as well through vertical advection of carbon-rich waters from the abyssal reservoir. However, quantification of this effect for highly idealized wind configurations using an earth system model yields only very small changes of atmospheric pCO_2 of roughly 5 ppmv (Menviel et al., 2008b). The nutrient supply via increased upwelling enhances biological productivity, which counteracts the effect of CO_2 release through increased ventilation of carbon-rich waters. In the MIROC experiments LGa and LGb, the Southern Ocean westerly winds weaken slightly over the sea ice area, but their position remains virtually unchanged. The simulated small westerly change under glacial climate states agrees well with other coupled AOGCM simulations in PMIP2 (Rojas et al., 2009). When estimating only the effect of the wind speed change on atmospheric pCO_2 through air-sea gas exchange, we find only a negligible contribution. It is difficult to quantify the impacts of wind-driven ocean circulation anomalies on atmospheric pCO_2 because of the complicated relationship between deep-water formation and deep upwelling.

6 Conclusions

A series of sensitivity experiments with a marine carbon cycle model forced by different glacial/interglacial climate scenarios was conducted to quantify the effects of climate dynamical changes on atmospheric CO_2 concentration. Our study extends previous studies using either box models (Köhler et al., 2005) or intermediate complexity models (Brovkin et al., 2007) in that it is based on fully coupled AOGCM results and an offline marine carbon cycle model similar to Tagliabue et al. (2009).

Atmospheric pCO_2 is relatively insensitive to 3-dimensional glacial ocean circulation changes as found in previous studies (Bopp et al., 2003; Tagliabue et al., 2009). Despite large AMOC differences in two LGM experiments, neither a weakening of NADW nor an increase of AABW formation causes a large change in atmospheric pCO_2. In this study, the shift of deep- and bottom-water formation from the North Atlantic to the Southern Ocean represents the dominant mode of Southern-origin carbon-rich bottom water in an abyssal ocean, but its effect on increased carbon pool is counteracted by the weakening of ocean carbon uptake by marine biota as shown by an increase in preformed phosphate. The reorganization of ocean circulation is not enough to account for the glacial atmospheric pCO_2 level.

Furthermore, the sea-ice extent plays different roles in modulating oceanic carbon distribution and hence atmospheric pCO_2 in two hemispheres. In the Northern Hemisphere, the sea-ice coverage increases atmospheric pCO_2 through less soluble CO_2, whereas the coverage in the Southern Ocean decreases the pCO_2 by inhibiting the degassing of DIC-rich deep water. This result adds another level of complexity to sea-ice-CO_2 feedbacks previously proposed by Stephens and Keeling (2000).

The ocean stratification associated with the weakening of NADW formation causes reductions both in surface DIC and alkalinity, thereby having only a small impact on the surface CO_2 concentration and atmospheric pCO_2. This simultaneous carbon chemistry changes might be due to the simplified biogeochemistry whereby the model assumes constant export rain ratio and settling rate of particles everywhere. The water temperature dependence of decomposition (Matsumoto, 2007) and calcification rate (Maier-Reimer and Bacastow, 1990) may add new sensitivities to the marine carbon cycle's response to LGM climate change that need to be further assessed in future work.

Acknowledgements. We would like to thank two anonymous external reviewers for helpful comments that substantially improved the manuscript. The numerical simulations were preformed on the Earth Simulator at JAMSTEC and HITACHI SR11000 at University of Tokyo. AT was sponsored through NSF grant 1010869.

Edited by: J. Singarayer

References

Adkins, J. F., Mcintyre, K., and Schrag, D. P.: The salinity, temperature, and $\delta^{18}O$ of the glacial deep ocean, Science, 298, 1769–1773, 2002.

Anderson, R. F., Ali, S., Bradtmiller, L. I., Nielsen, S. H. H., Fleisher, M. Q., Anderson, B. E., and Burckle, L. H.: Wind-driven upwelling in the Southern Ocean and the deglacial rise in atmospheric CO_2, Science, 323, 1443–1448, 2009.

Archer, D., Winguth, A., Lea, D., and Mahowald, N.: What caused the glacial/interglacial atmospheric pCO_2 cycles?, Reviews of Geophysics, 38, 159–189, 2000.

Archer, D., Martin, P. A., Milovich, J., Brovkin, V., Plattner, G.-K., and Ashendel, C.: Model sensitivity in the effect of Antarctic sea ice and stratification on atmospheric pCO_2, Paleoceanography, 18, 1012, doi:10.1029/2002PA000760, 2003.

Bacastow, R. B.: The effect of temperature change of the warm surface waters of the oceans on atmospheric CO_2, Global Biogeochem. Cy., 10, 319–333, 1996.

Bacastow, R. and Maier-Reimer, E.: Ocean-circulation model of the carbon cycle, Clim. Dynam., 4, 95–125, 1990.

Behrenfeld, M. J. and Falkowski, P. G.: Photosynthetic rates derived from satellite-based chlorophyll concentration, Limnol. Oceanogr., 42, 1–20, 1997.

Behrenfeld, M. J., O'Malley, R. T., Siegel, D. A., McClain, C. R., Sarmiento, J. L., Feldman, G. C., Milligan, A. J., Falkowski, P. G., Letelier, R. M., and Boss, E. S.: Climate-driven trends in contemporary ocean productivity, Nature, 444, 752–755, 2006.

Berger, A.: Long-term variations of caloric insolation resulting from the earth's orbital elements, Quaternary Res., 9, 139–167, 1978.

Bird, M. I., Lloyd, J., and Farquhar, G. D.: Terrestrial carbon storage at the LGM, Nature, 371, 566, doi:10.1038/371566a0, 1994.

Bopp, L., Kohfeld, K. E., and Le Quéré, C.: Dust impact on marine biota and atmospheric CO_2 during glacial periods, Paleoceanography, 18, 1046, doi:10.1029/2002PA000810, 2003.

Bouttes, N., Roche, D. M., and Paillard, D.: Impact of strong deep ocean stratification on the glacial carbon cycle, Paleoceanography, 24, PA3203, doi:10.1029/2008PA001707, 2009.

Bouttes, N., Paillard, D., and Roche, D. M.: Impact of brine-induced stratification on the glacial carbon cycle, Clim. Past, 6, 575–589, doi:10.5194/cp-6-575-2010, 2010.

Braconnot, P., Otto-Bliesner, B., Harrison, S., Joussaume, S., Peterchmitt, J.-Y., Abe-Ouchi, A., Crucifix, M., Driesschaert, E., Fichefet, Th., Hewitt, C. D., Kageyama, M., Kitoh, A., Laîné, A., Loutre, M.-F., Marti, O., Merkel, U., Ramstein, G., Valdes, P., Weber, S. L., Yu, Y., and Zhao, Y.: Results of PMIP2 coupled simulations of the Mid-Holocene and Last Glacial Maximum – Part 1: experiments and large-scale features, Clim. Past, 3, 261–277, doi:10.5194/cp-3-261-2007, 2007.

Broecker, W. S., Lynch-Stieglitz, J., Archer, D., Hofmann, M., Maire-Reimer, E., Marchal, O., Stocker, T., and Gruber, N.: How strong is the Harvardton-Bear constraint?, Global Biogeochem. Cy., 13, 817–820, 1999.

Brovkin, V., Ganopolski, A., Archer, D., and Rahmstorf, S.: Lowering of glacial atmospheric CO_2 in response to changes in oceanic circulation and marine biogeochemistry, Paleoceanography, 22, PA4202, doi:10.1029/2006PA001380, 2007.

Cameron, D. R., Lenton, T. M., Ridgwell, A. J., Shepherd, J. G., Marsh, R., and Yool, A.: A factorial analysis of the marine carbon cycle and ocean circulation controls on atmospheric CO_2, Global Biogeochem. Cy., 19, GB4027, doi:10.1029/2005GB002489, 2005.

Chikamoto, M. O., Matsumoto, K., and Ridgwell, A.: Response of deep-sea $CaCO_3$ sedimentation to Atlantic meridional overturning circulation shutdown, J. Geophys. Res., 113, G03017, doi:10.1029/2007JG000669, 2008.

Chikamoto, M. O., Matsumoto, K., and Yamanaka, Y.: Influence of Export rain ratio changes on atmospheric CO_2 and sedimentary calcite preservation, J. Oceanogr., 65, 209–221, 2009.

Crowley, T. J.: Ice age terrestrial carbon changes revisited, Global Biogeochem. Cy., 9, 377–389, 1995.

Curry, W. B. and Oppo, D. W.: Glacial water mass geometry and the distribution of $\delta^{13}C$ of $\sum CO_2$ in the western Atlantic Ocean, Paleoceanography, 20, PA1017, doi:10.1029/2004PA001021, 2005.

Dunne, J. P., Armstrong, R. A., Gnanadesikan, A., and Sarmiento, J. L.: Empirical and mechanistic models for the particle export ratio, Global Biogeochem. Cy., 19, GB4026, doi:10.1029/2004GB002390, 2005.

Duplessy, J. C., Shackleton, N. J., Fairbanks, R. G., Labeyrie, L., Oppo, D., and Kallel, N.: Deepwater source variations during the last climatic cycle and their impact on the global deepwater circulation, Paleoceanography, 3, 343–360, 1988.

Elderfield, H. and Rickaby, R. E. M.: Oceanic Cd/P ratio and nutrient utilization in the glacial Southern Ocean, Nature, 405, 305–310, 2000.

Eppley, R. W.: Temperature and phytoplankton growth in the sea, Fish. B.-NOAA, 70, 1063–1085, 1972.

Falkowski, P. G., Barber, R. T., and Smetacek, V.: Biogeochemical Controls and Feedbacks on Ocean Primary Production, Science, 281, 200–206, 1998.

Fischer, H., Schmitt, J., Luthi, D., Stocker, T. F., Tschumi, T., Parekh, P., Joos, F., Koheler, P., Volker, C., Gersonde, R., Barbante, C., Le Floch, M., Raynaud, D., and Wolff, E.: The role of Southern Ocean processes in orbital and millennial CO_2 variations – A Synthesis, Quaternary Sci. Rev., 29, 193–205, 2010.

Gent, P., Willebrand, J., McDougall, T. J., and McWilliams, J. C.: Parameterizing eddy-induced tracer transports in ocean circulation models, J. Phys. Oceanogr., 25, 463–474, 1995.

Gersonde, R., Crosta, X., Abelmann, A., and Armand, L.: Sea-surface temperature and sea-ice distribution of the Southern Ocean at the EPILOG Last Glacial Maximum – a circum-Antarctic view based on siliceous microfossil records, Quaternary Sci. Rev., 24, 869–896, 2005.

Gildor, H., Tziperman, E., and Toggweiler, J. R.: Sea ice switch mechanism and glacial-interglacial CO_2 variations, Global Biogeochem. Cy., 16, 1032, doi:10.1029/2001GB001446, 2002.

Hain, M. P., Sigman, D. M., and Haug, G. H.: Carbon dioxide effects of Antarctic stratification, North Atlantic Intermediate Water formation, and subantarctic nutrient drawdown during the last ice age: Disgnosis and synthesis in a geochemical box model, Global Biogeochem. Cy., 24, GB4023, doi:10.1029/2010GB003790, 2010.

Hesse, T., Butzin, M., Bickert, T., and Lohmann, G.: A model-data comparison of $\delta^{13}C$ in the glacial Atlantic Ocean, Paleoceanography, 26, PA3220, doi:10.1029/2010PA002085, 2011.

Hirst, A. C. and McDougall, T. J.: Deep-water properties and surface buoyancy flux as simulated by a z-coordinate model including eddy-induced advection, J. Phys. Oceanogr., 26, 1320–1343, 1996.

Ito, T. and Follows, M. J.: Preformed phosphate, soft tissue pump and atmospheric CO_2, J. Mar. Res., 63, 813–839, 2005.

Jahnke, R. A. and Jahnke, D. B.: Calcium carbonate dissolution in deep sea sediments: Reconciling microelectrode, pore water and benthic flux chamber results, Geochim. Cosmochim. Ac., 68, 47–59, 2004.

K-1 model developers: K-1 Coupled GCM (MIROC) Description, K-1 Technical Report No. 1, edited by: Hasumi, H. and Emori, S., K-1 Technical Report, 1, 34 pp., 2004.

Keeling, R. F., Stephens, B. B., Najjar, R. G., Doney, S. C., Archer, D., and Heimann, M.: Seasonal variations in the atmospheric O_2/N_2 ratio in relation to the kinetics of air-sea gas exchange, Global Biogeochem. Cy., 12, 141–163, 1998.

Key, R. M., Kozyr, A., Sabine, L., Lee, K., Wanninkhof, R., Bullister, J. L., Feely, R. A., Millero, F. J., Mordy, C., and Peng, T.-H.: A global ocean carbon climatology: Results from Global Data Analysis Project (GLODAP), Global Biogeochem. Cy., 18, GB4031, doi:10.1029/2004GB002247, 2004.

Kohfeld, K. E. and Ridgwell, A.: Glacial-interglacial variability in atmospheric CO_2, Surface Ocean-Lower Atmosphere Processes, Geophysical Research Series 37, Washington DC: American Geophysical Union, 251–286, 2009.

Kohfeld, K. E., Le Quéré, C., Harrison, S. P., and Anderson, R. F.: Role of marine biology in glacial-interglacial CO_2 cycles, Science, 308, 74–78, 2005.

Köhler, P., Fischer, H., Munhoven, G., and Zeebe, R. E.: Quantitative interpretation of atmospheric carbon records over the last glacial termination, Global Biogeochem. Cy., 19, GB4020, doi:10.1029/2004GB002345, 2005.

Kurahashi-Nakamura, T., Abe-Ouchi, A., Yamanaka, Y., and Mis-

umi, K.: Compound effects of Antarctic sea ice on atmospheric pCO_2 change during glacial-interglacial cycle, Geophys. Res. Lett., 34, L20708, doi:10.1029/2007GL030898, 2007.

Laws, E. A., Falkowski, P. G., Smith Jr., W. O., Ducklow, H., and McCarthy, J. J.: Temperature effects on export production in the open ocean, Global Biogeochem. Cy., 14, 1231–1246, 2000.

Levitus, S., Burgett, R., and Boyle, T.: World Ocean Atlas 1994 Volume 3: Nutrients, NOAA Atlas NESDIS 3, US Department of Commerce, Washington DC, 1994.

Louanchi, F. and Najjar, R. G.: A global monthly climatology of phosphate, nitrate, and silicate in the upper ocean: Spring-summer export production and shallow remineralization, Global Biogeochem. Cy., 14, 957–977, 2000.

Lund, D. C., Adkins, J. F., and Ferrari, R.: Abyssal Atlantic circulation during the Last Glacial Maximum: Constraining the ratio between transport and vertical mixing, Paleoceanography, 26, PA1213, doi:10.1029/2010PA001938, 2011.

Lynch-Stieglitz, J., Adkins, J. F., Curry, W. B., Dokken, T., Hall, I. R., Herguera, J. C., Hirschi, J. J.-M., Ivanova, E. V., Kissel, C., Marchal, O., Marchitto, T. M., McCave, I. N., MuManus, J. F., Mulitza, S., Ninnemann, U., Peeters, F., Yu, E.-F., and Zahn, R.: Atlantic meridional overturning circulation during the Last Glacial Maximum, Science, 316, 66–69, 2007.

Maier-Reimer, E. and Bacastow, R.: Modelling of geochemical tracers in the ocean, in: Climate-Ocean Interaction, edited by: Schlesinger, M. E., Kluwer Acad., Norwell, 233–267, 1990.

Marinov, I., Gnanadesikan, A., Sarmiento, J. L., Toggweiler, J. R., Floows, M., and Mignone, B. K.: Impact of oceanic circulation on biological carbon storage in the ocean and atmospheric pCO_2, Global Biogeochem. Cy., 22, GB3007, doi:10.1029/2007GB002958, 2008.

Martin, J. H.: Glacial-interglacial CO_2 change: The iron hypothesis, Paleoceanography, 5, 1–13, 1990.

Matsumoto, K.: Biology-mediated temperature control on atmospheric pCO_2 and ocean biogeochemistry, Geophys. Res. Lett., 34, L20605, doi:10.1029/2007GL031301, 2007.

Menviel, L., Timmermann, A., Mouchet, A., and Timm, O.: Meridional reorganizations of marine and terrestrial productivity during Heinrich events, Paleoceanography, 23, PA1203, doi:10.1029/2007PA001445, 2008a.

Menviel, L., Timmermann, A., Mouchet, A., and Timm, O.: Climate and marine carbon cycle response to changes in the strength of the Southern Hemispheric westerlies, Paleoceanography, 23, PA4201, doi:10.1029/2008PA001604, 2008b.

Oka, A., Kato, S., and Hasumi, H.: Evaluating effect of ballast mineral on deep-ocean nutrient concentration by using an ocean general circulation model, Global Biogeochem. Cy., 22, GB3004, doi:10.1029/2007GB003067, 2008.

Oka, A., Abe-Ouchi, A., Chikamoto, M. O., and Ide, T.: Mechanisms controlling export production at the LGM: Effects of changes in oceanic physical field and atmospheric dust deposition, Global Biogeochem. Cy., 25, GB2009, doi:10.1029/2009GB003628, 2011.

Oschlies, A. and Garcon, V.: An eddy-permitting coupled physical-biological model of the North Atlantic 1. Sensitivity to advection numerics and mixed layer physics, Global Biogeochem. Cy., 13, 135–160, 1999.

Otto-Bliesner, B. L., Hewitt, C. D., Marchitto, T. M., Brady, E., Abe-Ouchi, A., Crucifix, M., Murakami, S., and Weber, S. L.: Last glacial maximum ocean thermohaline circulation: PMIP2 model intercomparisons and data constraints, Geophys. Res. Lett., 34, L12706, doi:10.1029/2007GL029475, 2007.

Paillard, D. and Parrenin, F.: The Antarctic ice sheet and the triggering of deglaciations, Earth Planet. Sc. Lett., 227, 263–271, 2004.

Peacock, S., Lane, E., and Restrepo, J. M.: A possible sequence of events for the generalized glacial-interglacial cycle, Global Biogeochem. Cy., 20, GB2010, doi:10.1029/2005GB002448, 2006.

Peltier, W. R.: Global glacial isostasy and the surface of the ice-age Earth: The ICE-5G (VM2) Model and GRACE, Annu. Rev. Earth Pl. Sc., 32, 111–149, 2004.

Petit, J. R., Jouzel, J., Raynaud, D., Barkov, N. I., Barnola, J.-M., Basile, I., Bender, M., Chappellaz, J., Davis, M., Delaygue, G., Delmotte, M., Kotlyakov, V. M., Legrand, M., Lipenkov, V. Y., Lorius, C., Pépin, L., Ritz, C., Saltzman, E., and Stievenard, M.: Climate and atmospheric history of the past 420,000 years from the Vostok ice core, Antarctica, Nature, 399, 429–436, 1999.

Plattner, G.-K., Joos, F., Stocker, T. F., and Marchal, O.: Feedback mechanisms and sensitivities of ocean carbon uptake under global warming, Tellus B, 53, 564–592, 2001.

Robinson, L. F., Adkins, J. F., Keigwin, L. D., Southon, J., Fernandez, D. P., Wang, S.-L., and Scheirer, D. S.: Radiocarbon variability in the western North Atlantic during the last deglaciation, Science, 310, 1469–1473, doi:10.1126/science.1114832, 2005.

Rojas, M., Moreno, P., Kageyama, M., Crucific, M., Hewitt, C., Abe-Ouchi, A., Ohgaito, R., Brandy, E. C., and Hope, P.: The Southern westerlies during the last glacial maximum in PMIP2 simulations, Clim. Dynam., 32, 525–548, 2009.

Sarmiento, J. L. and Gruber, N.: Ocean Biogeochemical Dynamics, Princeton University Press, NJ, 526 pp., 2006.

Sarnthein, M., Winn, K., Jung, S. J. A., Duplessy, J., Labeyrie, L., Erlenkeuser, H., and Ganssen, G.: Changes in east Atlantic deep-water circulation over the last 30,000 years: Eight time slice reconstructions, Paleoceanography, 9, 209–267, 1994.

Sarnthein, M., Pflaumann, U., and Weinelt, M.: Past extent of sea ice in the northern North Atlantic inferred from foraminiferal paleotemperature estimates, Paleoceanography, 18, 1047, doi:10.1029/2002PA000771, 2003.

Schrag, D. P., Hampt, G., and Murray, D. W.: Pore Fluid constraints on the temperature and oxygen isotopic composition of the glacial ocean, Science, 272, 1930–1932, 1996.

Siegenthaler, U., Stocker, T. F., Monnin, E., Lüthi, D., Schwander, J., Stauffer, B., Raynaud, D., Barnola, J.-M., Fischer, H., Masson-Delmotte, V., and Jouzel, J.: Stable Carbon Cycle-Climate Relationship During the Late Pleistocene, Science, 310, 1313–1317, 2005.

Sigman, D. M. and Boyle, E. A.: Glacial/interglacial variations in atmospheric carbon dioxide, Nature, 407, 859–869, 2000.

Sigman, D. M., McCorkle, D. C., and Martin, W. R.: The calcite lysocline as a constraint on glacial/interglacial low-latitude production changes, Global Biogeochem. Cy., 12, 409–427, 1998.

Sigman, D. M., Hain, M. P., and Haug, G. H.: The polar ocean and glacial cycles in atmospheric CO_2 concentration, Nature, 466, 47–55, doi:10.1038/nature09149, 2010.

Skinner, L. C., Fallon, S., Waekbroeck, C., Michel, E., and Barker, S.: Ventilation of the deep Southern Ocean and deglacial CO_2 rise, Science, 328, 1147–1151, doi:10.1126/science.1183627, 2010.

Stephens, B. B. and Keeling, R. F.: The influence of Antarctic sea ice on glacial-interglacial CO_2 variations, Nature, 404, 171–174, 2000.

Tagliabue, A., Bopp, L., Roche, D. M., Bouttes, N., Dutay, J.-C., Alkama, R., Kageyama, M., Michel, E., and Paillard, D.: Quantifying the roles of ocean circulation and biogeochemistry in governing ocean carbon-13 and atmospheric carbon dioxide at the last glacial maximum, Clim. Past, 5, 695–706, doi:10.5194/cp-5-695-2009, 2009.

Toggweiler, J. R.: Variation of atmospheric CO_2 by ventilation of the ocean's deepest water, Paleoceanography, 14, 571–588, 1999.

Toggweiler, J. R., Murnane, R., Carson, S., Gnanadesikan, A., and Sarmiento, J. L.: Representation of the carbon cycle in box models and GCMs 2. Organic pump, Global Biogeochem. Cy., 17, 1027, doi:10.1029/2001GB001841, 2003.

Toggweiler, J. R., Russell, J. L., and Carson, S. R.: Midlatitude westerlies, atmospheric CO_2, and climate change during the ice ages, Paleoceanography, 21, PA2005, doi:10.1029/2005PA001154, 2006.

Wanninkhof, R.: Relationship between wind speed and gas exchange over the ocean, J. Geophys. Res., 97, 7373–7382, 1992.

Watanabe, M., Suzuki, T., O'ishi, R., Komuro, Y., Watanabe, S., Emori, S., Takemura, T., Chikira, M., Ogura, T., Sekiguchi, M., Takata, K., Yamazaki, D., Yokohata, T., Nozawa, T., Hasumi, H., Tatebe, H., and Kimoto, M.: Improved climate simulation by MIROC5: Mean states, variability, and climate sensitivity, J. Climate, 23, 6312–6335, doi:10.1175/2010JCLI3679.1, 2010.

Watson, A. J. and Naveira Garabato, A. C.: The role of Southern Ocean mixing and upwelling in glacial interglacial atmospheric CO_2 change, Tellus B, 58, 73–87, 2006.

Watson, A. J., Bakker, D. C. E., Ridgwell, A. J., Boyd, P. W., and Law, C. S.: Effect of iron supply on Southern Ocean CO_2 uptake and imlications for glacial atmospheric CO_2, Nature, 407, 730–733, 2000.

Weber, S. L., Drijfhout, S. S., Abe-Ouchi, A., Crucifix, M., Eby, M., Ganopolski, A., Murakami, S., Otto-Bliesner, B., and Peltier, W. R.: The modern and glacial overturning circulation in the Atlantic Ocean in PMIP coupled model simulations, Clim. Dynam., 3, 51–64, 2007.

Yamanaka, Y. and Tajika, E.: The role of the vertical fluxes of particulate organic matter and calcite in the oceanic carbon cycle: Studies using an ocean biogeochemical general circulation model, Global Biogeochem. Cy., 10, 361–382, 1996.

Yanase, W. and Abe-Ouchi, A.: The LGM surface climate and atmospheric circulation over East Asia and the North Pacific in the PMIP2 coupled model simulations, Clim. Past, 3, 439–451, doi:10.5194/cp-3-439-2007, 2007.